

HYDRODYNAMIC MODELS OF THE COLLISIONAL COMA

J.F. CRIFO
CNRS/IAS
BP 10
F91371 Verrières Cedex
France

ABSTRACT. The hydrodynamic approach to the modeling of the collisional regions of the cometary atmospheres is reviewed. A concise account of the existing Monte Carlo simulations is also incorporated. Emphasis is placed on works stimulated by the Halley flyby missions. The basic physical processes are described, based on the analogy with the physics of underexpanded jets. The general structure of the governing equations is presented and their legacy discussed. A detailed intercomparison is made of the application of these methods to the modeling of the comas. The reliability of the conclusions brought forward by existing models is discussed.

1. Introduction

In view of the extreme rarity of past and foreseeable in situ cometary missions, remote sensing of comets has been and will continue to be the essential tool of cometary investigation. Therefore, most properties (and, in particular, the statistical properties) of the solid nucleus of all comets have been and will continue to be inferred from observations of the cometary atmosphere—the coma. With the refinements of the observational techniques, a detailed and reliable understanding of the formation of the coma has emerged as a key objective of cometary physics.

The application of gas-dynamic methods to the formation of the coma seems to date only back to the year 1965. Fluid equations were first used in order to account for the acceleration of cometary dust and for the formation of many minor molecules. It is not a simple problem to delineate the precise extent of the collision-dominated part of a coma, i.e., that region where hydrostatic or hydrodynamic methods provide satisfactory results (see Sections 3.3 to 3.5). Primitive considerations, based on evaluations of the ratio of the local collision mean free path (m.f.p.) to the cometocentric distance, suggest that a water-dominated coma has a very small collision zone beyond an heliocentric distance ≈ 3 AU, while that zone covers the whole water survival zone within ≈ 0.5 AU (see, e.g., [13, 17]). The essential point, however, is that the distribution of matter in the coma, the dynamical properties of all constituents, and the chemical composition of the gas phase are

predominantly defined within a few hundred kilometers from the nucleus, that is, unquestionably, in a collision-dominated region, for all comets at least out to 3 AU from the Sun.

Progress in the development of hydrodynamic models of the coma was initially rather slow: based on [80], one can list about 25 works covering the period 1965 to 1982; in connection with the design and exploitation of the Halley flyby missions, the rate of publication in this field has increased by a factor of ≈ 5 , with more than 50 works analyzed here over the period 1983 to 1990. This is certainly because both the Halley flyby missions and new ground-based observational techniques have at last given direct (even though limited) access to the innermost collisionally dominated part of the coma.

The first phase of this increased hydrodynamic modeling effort has been extensively reviewed [31, 62]. Here, we put emphasis on the most recent developments. We first recall briefly the main goals of coma hydrodynamic models; next, we briefly indicate what the structure of an ideal model would be (Sections 3 to 6). We then attempt to qualify the present state of the art concerning a few key processes at work in the coma (Sections 7 to 12), and we conclude by trying to assess the reliability of present model results (Section 13).

2. Hydrodynamical Model Goals

Ideally speaking, a coma model should be a set of equations, based on physical assumptions, that would make it possible to derive from the whole body of coma “observations” the numerical values—with confidence intervals—of a number of physically significant parameters (e.g., the primary molecule and “primary dust” emission rate as a function of time at each position over the nucleus).

An essential property of such an ideal model would be its capability to fit all (or almost all) relevant observations. This is because any model, either primitive or very sophisticated, necessarily incorporates tens of adjustable parameters and makes choices among a large number of possible physical processes. It is therefore rather easy to fit any restricted set of observations. But this ease means that the confidence interval of most input parameters is nearly infinite. It usually means that the “nice agreement” boasted of by authors between restricted data and their model has only aesthetic value, because there presumably exists an immense variety of alternatives, and we cannot even be sure that their input assumptions would be compatible with the experimental values of other physical quantities that the model is not capable of taking into consideration.

What the existing works seem to have established is that the construction of such a comprehensive coma model (from which definitive conclusions could be produced) is a rather formidable task. We will devote the next sections to a presentation of the existing works considered as building blocks from which a final model will, we hope, appear in the future. We first wish to briefly summarize the various observational sets that are available or foreseeable for diagnostics of the collisional coma.

2.1. DUST

Local dust number density as a function of dust mass is available from in situ Halley flyby data and is expected from a few future flyby or rendezvous missions. Information on the global properties of the dust emission (distribution in space and velocities)

comes from remote sensing of the inner coma [9, 18], of the dust tail [27, 28], and of the dust trails [74] and from studies of the meteor streams [56, 64]. Limited information on the dust physicochemical composition comes from in situ results and from infrared spectrophotometry [18]. Detailed information on the dust emission patterns from the nucleus is available only in the case of P/Halley [41, 75, 76, 77].

2.2. NEUTRAL AND IONIZED GAS

The local number density, mass spectrum, and eventually flow velocity and temperature are available along the Giotto trajectory from in situ mass spectrometry [53, 83]. Most of the direct information on the primary molecule density, velocity, and temperature comes from high-resolution spectroscopy at infrared to radio wavelengths [6, 82]. Indirect constraints on the models come from spectroscopic studies of daughter molecules and ions, in general in the collisionless region of the coma, and from the study of the nongravitational forces [67].

3. Coma Hydrodynamic Model Structure

There is universal agreement that the coma originates from solar irradiation of the nucleus surface. The released gas and dust mixture expands freely into the solar wind, as the nucleus magnetic and gravitational fields are negligible. (However, the motion of very large grains in the vicinity of the nucleus is strongly influenced by the nucleus gravity field; also, the motion of the plasma in most of the coma is controlled by large-scale fields resulting from the solar wind flow past the comet.) This absence of binding forces definitely places the physics of the coma outside of the field of classical planetary aeronomy, where the presence of such forces is essential.

There is growing evidence that the gas-grain mixture is reactive, that is, that chemical reactions act among molecules, and that the dust undergoes transformations via fragmentation and/or gas-grain exchanges. The expansion of the mixture occurs under solar illumination, which powers the chemistry and heats (and perhaps alters) the grains. Described in this way, the formation of the coma may appear to be a very exotic and unique phenomenon deserving the development of entirely new methods. However, as occasionally mentioned in the past, and more insistently advocated recently [16, 20, 48], such is not the case. Expansion of a reactive dust-gas mixture into a rarefied ambient medium is nothing but what is called in rigorous hydrodynamic terms an underexpanded jet! Innumerable examples of underexpanded jets have been studied at the laboratory, in the industry, and even in Nature. The main peculiarities of the coma as a jet appear to be the intricate (and poorly known) initial conditions at the nucleus and the presence of solar illumination (however, many laboratory jets are currently operated under laser illumination). The huge size of the coma is not in itself a source of difficulty. Indeed, dimensional analysis indicates that, for instance, the coma of Comet Halley at the times of the flyby experiments was quite similar to currently operated laboratory water jets [16, 20].

The basic characteristic of an underexpanded jet is the rapid conversion of thermal energy into oriented energy, with the jet velocity usually becoming supersonic at eventually high Mach number values, and the jet temperature eventually decreasing to very small values. In the case of a coma, solar illumination triggers a wealth of exothermic photochemi-

cal reactions. Accordingly, the gas temperature has a complex altitude profile, going first through a minimum, then increasing again until a secondary maximum is reached [23].

If the source is very inhomogeneous, one is faced with the interaction of a number of primary jets, which implies the formation of a pattern of shock structures. At this time, however, this problem has been approached only once [47], and we will here mostly consider a single-jet coma as would be produced by a "smooth" nucleus.

3.1. LOCAL THERMAL EQUILIBRIUM AND RELAXATION

One of the properties of underexpanded jets that plays an essential role in the case of the coma is the breakdown of local thermal equilibrium (LTE) associated with the fast decrease of the density with distance to the nucleus (approximately proportional to the inverse square, as verified *in situ* [53]). Accordingly, the various degrees of freedom that describe the jet gradually behave separately from one another. For instance, the velocity and temperature of dust grains with different masses separate from one another and from those of the gas [31, 62, 66, 80], the gas phase chemical composition departs from chemical equilibrium values [35], the vibrational and rotational level population of each molecule deviate from Boltzmann equilibrium at the kinetic temperature of the molecule [6, 24], and even the thermal velocity distribution of each species ceases to assume a Maxwell-Boltzmann form [2, 3, 8, 10, 33, 73, 79]. When complete uncoupling of all degrees of freedom is achieved, one is in the collisionless region of the coma. It is a fundamental requirement of coma models to properly allow for these effects, because most observable quantities involve relaxing degrees of freedom (e.g., the mass dependence of the dust velocity and temperature, the rotational structure of a molecule emission band, and the mass spectrum of a gas volume element). Also, at any point in the collisional coma, part of the degrees of freedom turns out to be relaxing (e.g., the dust and the fast dissociation products are nowhere in complete thermal equilibrium with the gas).

3.2. CATASTROPHIC EFFECTS

A medium under non-LTE conditions is, by definition, unstable and susceptible to a catastrophic return to equilibrium. One example, well-documented in laboratory jets and in Nature, is recondensation of a supercooled vapor into a fog. In the case of a water-dominated coma, due to the mentioned expansion cooling of the coma, the local water pressure quickly exceeds by large factors the equilibrium sublimation pressure of ice at the local temperature. As a consequence, it has been pointed out [17, 21, 39, 44] that catastrophic formation of water clusters is expected.

Another example follows from the fact that a certain number of molecular level populations are inverted in part of the coma: this leads to maser emission. However, at least in the case of water, it has been shown that the effect is marginal [6, 24].

3.3. THE COLLISION SPHERE PARADIGM

Current experience acquired on underexpanded jets reveals (e.g., [3, 10, 79]) that, following the smoothness of the density decrease along the flow direction, the various relaxations are continuous processes. Accordingly, the gas dynamic treatment is usually done in three successive steps:

1. The fluid region, where fluid equations are applicable, because the gas velocity distribution function (d.f.) differs only very slightly from its equilibrium Maxwell-Boltzman shape.
2. The transition region, where the d.f. is no longer Maxwellian, but where the effect of collisions is not negligible. In principle, the collisional Boltzman Equation (CBE) must be used there, but since it is intractable, various approximate simpler forms of the CBE are used [8, 10, 73, 79].
3. Finally, when collisions are negligible, the collisionless Boltzman equation (or Liouville equation) can be used.

A radically different approach (nonanalytic) to the modeling of a nonequilibrium flow, which has received considerable developments in other contexts, is the direct Monte Carlo (DMC) simulation ([63]; see also [2, 5, 33, 34]). It has recently been proven capable of dealing with chemically reacting and radiating rarefied flows and, in the future, may prove to be the reference method against which analytic methods will be calibrated. At the present time, DMC simulations of the nucleus coma interface [5] and of a pure water coma (subject to photodissociation) have appeared [33, 34]. We do not review these works in detail here, but we will make ample use of their results in various sections.

For historical reasons, the construction of hydrodynamic coma models has not been based on the methods developed for jets, but on a more or less arbitrary transfer of planetary aeronomy concepts. There, owing to the dominance of gravity, the atmosphere is in hydrostatic (not hydrodynamic) equilibrium. Its density decreases exponentially with altitude, and as a result, the transition region (in the above sense) is of negligible extent: one can separate the medium into a collision sphere and a collisionless exosphere. Notwithstanding this essential difference between a planetary atmosphere and a coma, many cometary authors have adopted the concept of a "collision sphere." They define it as the region where the ratio K of the local m.f.p. Λ to the cometocentric distance r (which is the characteristic length for a power law decrease in density) is smaller than unity [11, 13, 26, 37, 40, 70]. (In the gas dynamic context, K is called the "Knudsen number.") It is, for instance, assumed that all gaseous constituents assume a constant velocity outside of this sphere, and so on. Other authors, however, use fluid equations throughout the coma, sometimes expressing uneasy feelings about doing so.

Before coming back on this problem, it may be enlightening to draw attention to results from the first DMC simulation of a water coma achieved recently [33]. This will illustrate the problem quite convincingly.

3.4. THE DIRECT MONTE CARLO SIMULATION APPROACH

DMC simulation is one of the tools by which the dynamical properties of a non-equilibrium gas can be reproduced (e.g., [2]). It was first introduced in the cometary context to derive the distribution function of the fast dissociation products of H_2O , H , and OH [7, 12, 13, 40, 43], with the assumption that the outflowing water was in local thermal equilibrium. This approach could be called a "mixed Monte Carlo-hydrodynamic approach." We do not review it here, although we will quote some of the results later on. Recently, results have been reported [33] of a "full" DMC simulation, that is, in which the distribution of all constituents, including H_2O itself, is derived. Halley flyby conditions

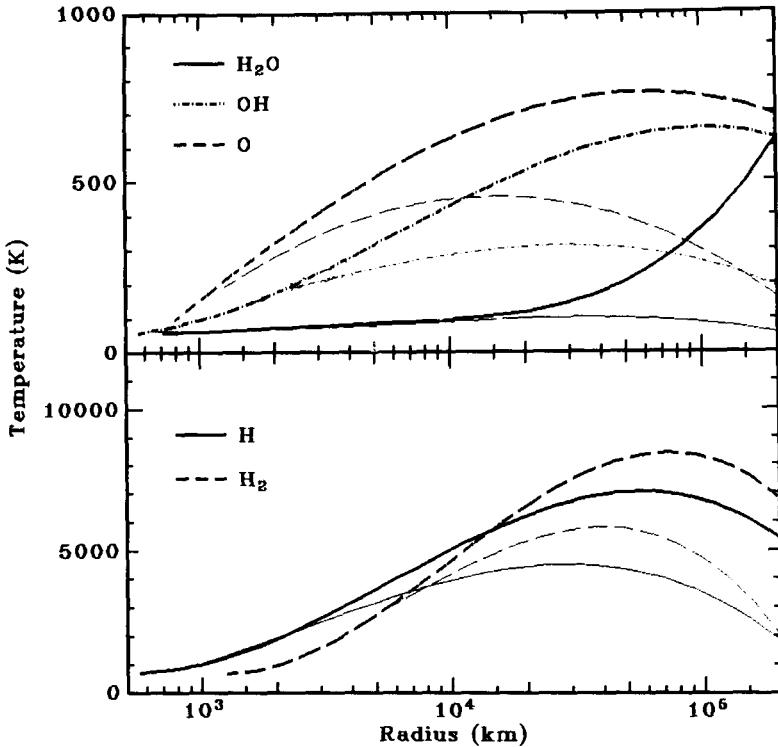


Figure 1. Parallel (heavy lines) and perpendicular (thin lines) temperature profiles for the five main components of a pure water coma, as obtained from a full Monte Carlo simulation with parameters appropriate for Halley flyby conditions. From [33].

are postulated. Figure 1 shows some of the results, which reveal the following classical behavior observed in laboratory jets (e.g., [2, 10] and Figure 2):

1. The velocity d.f. of all constituents considered becomes increasingly nonspherical with altitude. If an ellipsoidal approximation is used for the d.f., the water parallel temperature T_{\parallel} decreases at high altitude (as in the case of adiabatic expansion), while the transverse temperature T_{\perp} “freezes out” and (here) increases out to the limit of the computational domain (2×10^5 km).
2. The departure from sphericity of the d.f. is gradual, and does not display a sharp discontinuity at an altitude that could be called the “boundary of the collision sphere.”

Below, we will briefly comment on the results of two other recent DMC simulations of the water outflow, which have investigated the nucleus-coma interface region [5] and the preservation at high altitudes of gas production inhomogeneities [34].

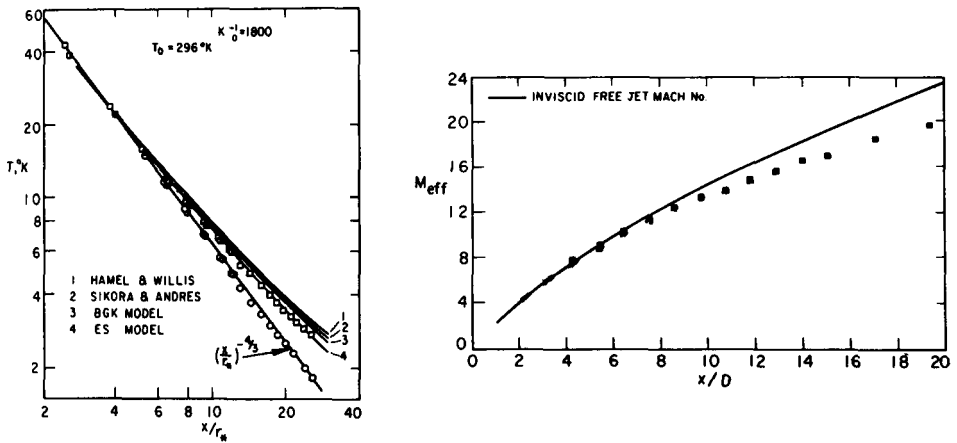


Figure 2. Free-jet expansion of helium with an initial Knudsen number K_0 similar to that at the base of Comet Halley [10]. Left: Parallel (\square) and transverse (\circ) temperatures as a function of normalized distance. The parallel data are fitted with an adiabatic expansion law, while the transverse ones are compared with various modified CBE models (labeled 1 to 4). Right: Effective Mach number as a function of normalized distance (\blacksquare) compared with an inviscid model computation. A viscous model (not shown) provides an almost perfect fit.

The cited DMC simulations do not incorporate radiative effects. Nonetheless, their results demonstrate the power of DMC methods to deal with a coma. However, it should be clear that there are practical limitations to their use, associated with computer resources requirements. Thus, it would appear sensible to use these techniques only when analytic methods definitely do not exist. This brings us back to the question of the range of validity of fluid equations and to the possible alternative methods.

3.5. LEGACY AND USEFULNESS OF THE HYDRODYNAMIC APPROACH

The most critical relaxation effect is translational relaxation (i.e., departure of the d.f. from Maxwellian shape). This is because all other relaxations can be relatively well treated by rate equations, if the d.f. is Maxwellian (the rate coefficients having, in this case, generally well-understood expressions). While the acceleration of the dust and the production of most minor molecules unquestionably occur in a fluid zone, the formation of the collisionless coma of daughter molecules and the equilibration of the internal modes of the molecule occur mostly in regions where translational relaxation is at work. At the present time, this effect has not been allowed for by the use of modified CBEs. Instead, the bulk velocity and an “effective” local temperature are computed by fluid equations by some of the authors, while the others “freeze” their value at the boundary of “the collision sphere”

($K = 1$). Based on DMC simulations [33] and comparison between theory and laboratory experiments [8, 10, 65, 79], the situation can be qualified as follows:

1. The temperature and velocity do not freeze out at $K \approx 1$, but, at best, at $K = 10$.
2. The velocity d.f. ceases to be Maxwellian at $K \approx 0.1$, not $K \approx 1$. This defines the validity range of fluid equations.
3. In the transition region $0.1 < K < 10$ (most of the observable coma at 1 AU from the Sun), viscous fluid equations provide generally usable results, in the sense that the computed velocity and temperature acceptably approximate the experimental data. As stated in [79], “the range of usefulness of a good theory exceeds its range of legacy,” and this is precisely the case for the Navier Stokes Equations (NSEs), which are the most widely used viscous fluid equations. Figure 2 shows one example in support of this statement, but many others can be found in the quoted literature.

We tentatively conclude that for modeling most of the coma, until appropriate CBE methods are available, it is convenient to use a multifluid approach. Speculations based on the collision sphere concept are a priori unwarranted.

3.6. THE MULTIFLUID APPROACH

The coma is considered here as a multiphase multispecies fluid. In order to minimize the number of governing equations, the components that share common flow parameters (V and T) are grouped together into elementary fluids. This subdivision is, in principle, a delicate procedure to be based on an evaluation of the mutual equilibration scale lengths of the components [62]. At the present time, the situation is as follows:

1. The primary molecules and all daughter molecules that are produced in negligibly excited states (that is, with small excitation energy and excess velocity) are considered to make up a single fluid sharing a common flow velocity V_g and temperature T_g . Both V_g and T_g are computed by hydrodynamic equations [7, 12, 13, 15, 18, 21, 22, 23, 24, 29, 30, 36, 40, 42, 44, 45, 46, 47, 49, 50, 51, 52, 57, 58, 59, 69, 71, 78].
2. The rotational and vibrational excitation of the molecules and the detailed chemical composition, when computed, are derived by a nonequilibrium method, i.e., by rate equations [1, 6, 24, 36, 69, 83].
3. The daughter molecules produced in highly excited states or with larger excess velocities (e.g., H) are treated by heuristic quasi-fluid equations [35, 36, 37, 38, 58, 59, 62, 69, 83] or by Monte Carlo simulations [7, 12, 13, 40, 43].
4. The ions (which are all daughter molecules) are either incorporated into the main fluid or treated by separate hydrodynamic equations [51, 57].
5. The electrons are either incorporated into the main fluid or treated by independent fluid equations [35, 51, 57, 58, 59, 60, 69, 83].
6. The dust, if taken into account, is treated as a fully relaxed population (i.e., with zero kinetic temperature and with mass-dependent bulk velocity and internal temperature). In some models, the dust is approximated by particles of a

- single size. In other models, it has a broad size spectrum [18, 29]. Chemically speaking, some models assume a single species, while others assume a mixture of species (e.g., [15, 18]). In one instance, icy grains have been incorporated [15]. Pioneering efforts to allow for pyrolysis and fragmentation effects have recently appeared [42, 81].
7. Water recondensation, when taken into account, has been treated by the semi-heuristic classical homogeneous nucleation theory [17, 21, 39, 44], i.e., the very small water clusters (typically with less than 10 molecules) are incorporated into the main fluid, while the large clusters (with up to 1000 molecules per cluster) are treated as a fully relaxed single-size population with altitude-dependent grain size.
 8. The radiation field (line and continuum) is computed by radiation transfer methods [6, 24, 57, 59, 60, 68].

An ideal model of the coma should incorporate the treatments listed above to an ultimate level of detail: for instance, the excitation state of all important molecules should be treated, and the full mass spectrum of the dust should be incorporated. Besides this, effects not yet comprehensively treated should also be included (e.g., dust fragmentation and dust pyrolysis). Finally, an ideal model should take into consideration realistic boundary conditions at the nucleus surface, not only from the point of view of the physics of the dust and gas release [4, 17, 67, 72], but also with respect to the inhomogeneity of the nucleus surface and to the nucleus shape and rotation [41].

In practice, all existing models incorporate only a fraction of the preceding capabilities. As an example of prototype integrated models, one can look at [57, 60].

Aside from their physical description of the coma, existing models differ in the details of the fluid equations they incorporate (Section 4) and in their mathematical sophistication (geometry and capacity of dealing with time-dependent effects). But they are ultimately all differing variants of a unique formalism, i.e., a set of coupled inhomogeneous NSEs supplemented by coupled rate equations. We now briefly describe their common building blocks: the single fluid equation and the rate equation.

4. Fluid Equations

In a coma, LTE conditions do not exist, since they would require that all fluids share a common velocity and temperature, and that the radiation field be a blackbody field at that temperature. However, it is hoped that as long as mutual collisions within a fluid dominate its d.f., LTE equations can be used for it, irrespective of the mentioned globally non-LTE conditions. These equations must, however, allow for the existence of the other fluids.

Fluid equations for an isolated single fluid are obtained by taking velocity moments of the CBE up to a certain order and dropping the terms that involve moments of higher order [8, 79]. It can be shown that the greater the departure of the local d.f. from Maxwellian shape, the greater the cutoff order must be. In the LTE region, five moments are sufficient: one obtains the familiar inviscid approximation “mass, momentum, and energy” (MME) equations. The NSEs make up the next consistent approximation, incorporating viscous dissipation and heat conduction, the two first-order effects associated with a distortion of the d.f. (see the concise introduction to the NSEs in [20], and extensive de-

velopments in, e.g., [8]). There exist higher order equations, which are suitable for large departures of the d.f. from Maxwellian shape, but because in our case these departures would result from the rarity of collisions, it is probably easier to use, as already mentioned, simplified CBE equations instead of high-order moment equations [8, 79].

The NSEs applicable to an isolated monoatomic gas have been derived rigorously and are mathematically homogeneous; in order to incorporate the exchanges between flow parameters and internal degrees of freedom in a polyatomic gas, they are heuristically generalized by adding "inhomogeneous" terms. If the fluid (i) is a component of a multifluid mixture, other terms are added representing, in a more or less rigorous way, its interactions with the other fluids (j) and with the radiation field (r).

At the present time, the NSEs have been used to compute the two-dimensional structure of a cylindrical pure water coma [46]. Unfortunately, the solution was not looked for at high altitudes, where the superiority of the NSEs over the MME equation should manifest itself. NSEs have also been used to compute the properties of electrons and ions in the innermost coma (see Section 11). We do not reproduce here the full form of the compressible NSE; the interested reader is referred to [8, 20, 45, 46, 65, 79]. All other works use the inviscid MME approximation (without explicit justification).

In the MME approximation, the moment equations expressing the conservation of mass, momentum, and energy read:

$$\frac{\partial \rho_i}{\partial t} + \nabla \cdot (\rho_i \mathbf{V}_i) = \sum_j \dot{M}_{ij} \quad (1)$$

$$\frac{\partial M_{ij}}{\partial t} (\rho_i \mathbf{V}_i) + \nabla \cdot (\rho_i \mathbf{V}_i \mathbf{V}_i) + \nabla p - \mathbf{E}_i = \sum_j (\dot{P}_{ij} + \dot{M}_{ij} \mathbf{V}_j) + \dot{P}_{ir} \quad (2)$$

$$\frac{\partial}{\partial t} (\rho_i e_i) + \nabla \cdot [(\rho_i e_i + p) \mathbf{V}_i] - \mathbf{E}_i \cdot \mathbf{V}_i = \dot{E}_{ir} + \sum_j (\dot{E}_{ij} + \dot{P}_{ij} \cdot \mathbf{V}_j + \dot{M}_{ij} V_j^2 / 2) \quad (3)$$

with the following definitions: ρ_i is the mass density, \mathbf{V}_i , the bulk velocity vector, p , the total kinetic pressure, e_i , the total internal energy, \mathbf{E}_i , the external force field, M_{ij} , P_{ij} , and \dot{E}_{ij} , the rate of mass density, momentum density, and energy density exchanges with fluid (j), and \dot{P}_{ir} and \dot{E}_{ir} , the rates of momentum and kinetic energy density exchanges with the radiation field (r). For perfect gases:

$$p = \sum_j \rho_j k_B T_j / m_j \quad (4)$$

where k_B is Boltzman's constant, m_j is the molecules' mass, and T_j is the temperature. Finally, for a polyatomic perfect gas at LTE:

$$e_i = h_i + (1/2) V_i^2 - k_B T_i/m_i \quad (5)$$

with h_i , the specific internal energy, being given by:

$$h_i = \gamma_i/(\gamma_i - 1) (k_B T_i/m_i) \quad (6)$$

where γ_i is the molecule specific heat ratio C_p/C_v . Since LTE is assumed, one has:

$$\gamma_i = (d_i + 5)/(d_i + 3)$$

where d_i is the number of internal degrees of freedom in thermal equilibrium at the temperature T_i ; d_i can assume noninteger values to allow for the fact that at any temperature, only some of the excitation levels of a given degree of freedom may perhaps be excited. But those degrees of freedom that are excited, but not in thermal equilibrium at T_i , should be excluded from d_i .

Table 1 lists the various fluids that can be found in existing coma models.

Let us remark that some zero (kinetic) temperature fluid are in use: for instance, a fluid of fast prethermal H atoms [58, 62], the fluid of single-size dust grains, and the fluid of large water clusters. They are governed by equations (1) to (6), where:

$$T_i = p_i = h_i = \dot{E}_{ij} = \dot{E}_{ir} = 0.$$

The derivation of expressions for the inhomogeneous terms of the NSEs constitutes a difficult task. We discuss some examples in Sections 7 to 11.

5. Rate Equations

The purpose of these equations is to compute the numerical values of the internal parameters of each fluid. Examples are the rotational level population P_{jk} of a certain molecule (j), the mole fractions x_{jk} that describe the abundance of the molecule (k) within the fluid (j), and the size distribution $n(a)$ of the water clusters produced by recondensation.

The rate equations are conservation laws that express the net budget of all transitions between the accessible states for each internal parameter. These expressions involve rate coefficients that are usually functions of the fluid temperature. For that reason, all components of a given fluid (j) must share a common flow velocity and kinetic temperature. (As a counter-example, coma dust cannot form a single fluid, because each grain size assumes its own velocity.)

5.1. RATE EQUATIONS FOR THE LEVEL POPULATIONS

Rate equations express the net budget of the transitions that are induced by collisions or radiation and that spontaneously occur. Introducing the state-to-state relaxation rate coefficients $K_{jj'}$, the Einstein coefficients for spontaneous emission $A_{jj'}$ and the

Table 1. General Structure of Recent Multifluid Models of the Coma

<u>Elementary Fluids Treated</u>	<u>References</u>
Pure water	6, 7, 11, 15, 17, 18, 21, 23, 24, 29, 30, 33, 40, 44, 45, 46, 50, 51, 52, 78
Heavy neutrals and ions	1, 12, 13, 35, 36, 47, 58, 59, 60, 69, 71
Ions	14, 51, 57
“Fast” atomic hydrogen	33, 58, 69
“Thermal” atomic hydrogen	33
Electrons	14, 35, 46, 51, 57, 58, 59, 69
Single-size dust	12, 15, 17, 18, 21, 23, 29, 30, 45, 46, 47, 52, 57, 59, 60
Large water clusters	17, 21, 23, 44
Icy grains	15
<u>Heavy Fluid Internal Parameters</u>	
Several chemical species	1, 12, 13, 35, 36, 47, 51, 57, 58, 59, 60, 69
Several excitation levels	6, 7, 23, 24, 57, 60
<u>Radiation Field Computations</u>	
Optically thin equations	35, 36, 69
Broad-band radiative transfer	57, 58, 59, 60
Line-by-line transfer	6, 7, 23, 24
<u>Mathematical Capabilities</u>	
Spherical coma	All, except 45, 46, 50, 52, 78
Cylindrical coma	45, 46, 50, 52, 78
Three-dimensional coma	47
Time-stationary coma	All, except 30, 45, 46, 50, 52, 78
Time-dependent coma	30, 45, 46, 50, 52, 78
<u>Main Goal of the Work</u>	
Illustrative	All, except 1, 6, 12, 18, 21, 23, 29, 33, 40, 71
Quantitative fit to observations	1, 6, 12, 18, 21, 23, 29, 33, 40, 71

Einstein coefficients for induced transitions $B_{jj'}$ (where j and j' are two levels), we write [6, 24]:

$$\frac{\partial P_j}{\partial t} + \nabla \cdot (P_j \underline{V}_j) = \sum_j (K_{j'j} P_{j'} - K_{jj'} P_j) + \sum_{j' > j} P_{j'} A_{jj'} - \sum_{j' < j} P_{j'} A_{jj'} + \sum_{j' \neq j} (P_{j'} B_{j'j} - B_{jj'} P_j) u(\lambda_{jj'}) \tag{8}$$

in which $u(\lambda_{jj'})$ is the radiation density at the wavelength $\lambda_{jj'}$ of the transition. The above sums are, of course, restricted to allowed transitions. Microbalance and Einstein relations can be used to express all coefficients in the right-hand side (r.h.s.) as a function of the $K_{jj'}$ and $A_{jj'}$ only. The forms of these coefficients are harder to assess, and presently, in the cometary context, semiheuristic expressions are in use. Finally, notice that the $K_{jj'}$ may involve several fluids (e.g., excitation or quenching of a molecule by electrons).

5.2. CHEMICAL COMPOSITION

The conservation equations for a species (s) taking part in N_R reactions involving N_P other products have the general form [69]:

$$\frac{\partial n_s}{\partial t} + \nabla \cdot (n_s \underline{V}_s) = \sum_{s'=1}^{N_R} v_{ss'} k_{s'} n_1^{m_{1s'}} \dots n_{N_P}^{m_{N_P s'}} \tag{9}$$

where $v_{ss'}$ is the stoichiometric coefficient (≥ 0), $m_{ss'} = \sup(v_{ss'}, 0)$ is the reaction order, $k_{s'}$ is the reaction rate, and n_s is the species concentration. Equation (9) eventually incorporates photochemical reactions, in which case, k_s involves the local radiation field. But they cannot properly represent reactions between distinct fluids with differing temperatures. In this case, special formalisms must be developed.

5.3. DUST TEMPERATURE

The fluid that groups all spherical dust grains with the same mass m_d is considered to have negligible kinetic temperature, but has a variety of internal temperatures T_d^k if there is a distribution of mineral composition. It can be shown that the velocity dispersion introduced by any reasonable temperature spread is negligible: therefore, the single fluid concept is acceptable. The rate equation for T_d^k is:

$$m_d C_d^k \left[\frac{\partial T_d^k}{\partial t} + \nabla \cdot (T_d^k \underline{V}_d) \right] = \dot{E}_{abs}(a_d, r) - \dot{E}_{rad}(a_d, T_d^k) + \dot{E}_{conv}(T_d^k, \underline{V}_d) \tag{10}$$

where \underline{V}_d is the grain velocity, a_d the grain radius, C_d^k the grain specific heat content, E_{abs} the energy deposition rate from the local radiation field, E_{rad} the energy loss rate by thermal

emission (see Section 7.2), and \dot{E}_{conv} the gas grain convective energy exchange rate (the explicit form of this term can be found, e.g., in [17]).

5.4. ICY GRAIN AND WATER CLUSTER SIZE AND TEMPERATURE

A collection of icy grains with identical initial size, shape, and mass can be considered as a zero kinetic temperature fluid with position-dependent size and internal temperature. Similarly, it can be shown that the large clusters formed by recondensation have a negligible size dispersion [21, 44]. Assuming spherical shape, the rate equations for temperature and radius are [15, 17, 44]:

$$m_c C_c \left[\frac{\partial T_c}{\partial t} + \nabla_c \cdot (T_c \underline{V}_c) \right] = \dot{E}_{\text{abs}}(a_c, r) - \dot{E}_{\text{rad}}(a_c, T_c) + \dot{E}_{\text{conv}}(T_c, \underline{V}_c) + \dot{E}_{\text{exch}}(T_c, \underline{V}_c) \quad (11)$$

$$4\pi a_c^2 \rho_c \left[\frac{\partial a_c}{\partial t} + \nabla_c \cdot (a_c \underline{V}_c) \right] = \dot{M}_{\text{exch}}(T_c, \underline{V}_c) \quad (12)$$

where the symbols have the same meaning as before, and ρ_c is the specific mass, E_{exch} is the net energy budget of recondensation on the grains and sublimation from the grains, and M_{exch} is the corresponding net mass budget. The explicit form of these terms is given in [17, 44].

6. Radiative Transfer Equations

Knowledge of the radiation field at every point in the coma is needed for the assessment of the dust temperatures, of the molecules' internal excitation state, and of the photochemical rates. The local radiation field at any point in the coma is predominantly direct solar light, but, in the vicinity of the nucleus surface, emission from the nucleus (especially the hot inactive sunlit regions) and from dark dust may dominate at infrared (IR) wavelengths. The emission from the molecules and dust grains is, of course, that part of the radiation field that carries the greatest information on the coma. Light propagating across the coma is subject to absorption and scattering by the dust and by the molecules.

6.1. RADIATIVE TRANSFER IN THE CONTINUUM

At ultraviolet (UV) wavelengths, pure absorption is caused predominantly by the molecular photodissociation and ionization, with dominance of the H₂O continuum. It can be accounted for by the simple expressions:

$$F_\lambda(r) = F_\lambda(\infty) \exp[-\tau_\lambda(r, \infty)] \quad (13)$$

with

$$\tau_\lambda(r_1, r_2) = \sum_j \{[\sigma_j(\lambda)/m_j] \int_{r_1}^{r_2} \rho_j(r') dr'\} \tag{14}$$

where σ_j (cm²) is the differential cross-section at wavelength λ , F_λ is the solar radiation flux, the integration is to be performed along the line of sight, and the summation is to be performed over the most abundant molecules [31, 35, 62]. At typical coma production rates, the effect is only important within some 100 km from nucleus surface and has consequences mostly on the gas phase chemistry. An iterative computation is therefore needed to consistently assess the effect.

At visible and IR wavelengths, absorption, scattering, and thermal emission by the dust are the dominant sources of radiation transfer. The effect is to attenuate the direct solar light and to build up a diffuse radiation field, with consequences to the nucleus production rate, the dust temperature, and the molecule excitation state [59, 68]. In first approximation, the optically thin approximation is used with the attenuation given by (13) but with

$$\tau_\lambda(r_1, r_2) = \sum_k \int_0^\infty da_d \left[\pi a_d^2 Q_E^k(\lambda, a_d) \int_{r_1}^{r_2} n_d^k(r', a_d) dr' \right] \tag{15a}$$

where Q_E is the Mie extinction efficiency, n_d is the dust number density at radius a_d and position r' , the summation is carried over the different dust chemical classes, and the integration is performed over the size distribution and the line of sight. The single scattering diffuse radiation field is given by:

$$f_\lambda(r) = \sum_k \int \int \int \int \pi a_d^2 n_d^k(r', a_d) \{Q_S^k(a_d, \lambda) \varpi^k(a_d, \lambda) F_\lambda(\infty) \times \exp[-\tau_\lambda(r', \infty)] + Q_A^k(\lambda) B_\lambda [T_d^k(a_d, r')]\} \exp[-\tau_\lambda(r, r')] da_d dr' d\Omega(r') \tag{15b}$$

where Q_S^k and Q_A^k are the Mie scattering and absorption efficiency, ϖ_k is the Mie scattering phase function, B_λ is the Planck function, τ_λ is given by (15), Ω is the elementary solid angle from r to r' , and T_d^k is computed from (10). The implicit assumption of spherical grain shape is consistent with the assumption of sphericity made for computing the hydrodynamic interaction of the grains. It has also a physical justification, since nonspherical grains will be spinning fast due to hydrodynamic torques [18].

Optical thickness effects are possibly important only at wavelengths smaller than the size a_*^k where the function $a^2 n_d^k(a)$ peaks, because for $\lambda \gg a_*^k$, the extinction follows Rayleigh equations. Therefore, equation (15) (with $\tau_\lambda \approx 0$) correctly gives the diffuse field at infrared wavelengths. Furthermore, in this case, because of the high dilution of the solar light, the scattered term can be ignored in (15). At visible wavelengths, because of the small grain temperatures, the thermal emission can be ignored in (15), but $\tau_\lambda \neq 0$.

The treatment of the optically thick case is a formidable task, in particular, because of the complex variation of ω^k with size. Various approaches have been made ([59], [68], and references therein). The most recent contribution is a Monte Carlo simulation [68]. It indicates that, for our present problem, opacity effects are not very important, even at production rates in excess of 10^{30} molecules/s: even at the nucleus surface (on the dayside), the energy input is reduced by less than 30%, and more likely less than 10%. This has been spectacularly evidenced by the sharpness of the Giotto images (with the possible exception of a very limited limb region [41]). Most earlier results indicating a strong effect have been shown to incorporate either errors or inadequate assumptions [68].

6.2. RADIATIVE TRANSFER IN THE LINES

Because of the small coma gas temperature, the small collision rates, and the fact that parent molecules fluoresce only at infrared wavelengths, these molecules are generally vibrationally relaxed and have a small number of excited rotational lines. In the case of water, the theoretical predictions [6, 24] have been spectacularly confirmed by observations [82]. Due to the small number of populated levels and to the relatively high density of water in the coma, a certain number of the lines are optically thick [6, 24]. While the number of populated levels is small, the total number of levels to be a priori incorporated into the rate equations (8) is large; therefore, it is impracticable to solve exact transfer equations. Instead, one has to use approximating methods (e.g., the escape probability method applicable in a spherically symmetric coma [6, 24]), which provide closed-form expressions to be incorporated into the rate equations. Typically, it is found that many rotational transitions of water are optically thick throughout the coma.

An attempt at estimating an effective IR radiative field in the H₂O bands by solving a simpler band-integrated radiation transfer equation has also been made [60], but the results have proven not to be in agreement with the more exact line-by-line treatment (see Section 9.2).

7. Gas-Dust Interaction

This subject has been treated in detail in previous reviews [31, 62, 80]. Multi-dimensional gas-dust interactions are reviewed by T.I. Gombosi in this book. We therefore treat this topic in a concise form here.

Practically all present models follow the pioneering treatment [66] in which the dust is represented by spherical grains and their interaction with the gas is represented by classical free molecular "convective exchange" terms. It has been suggested [60] that efficient coupling between gas and dust in the innermost coma occurs also via the infrared dust emission. We come back to this in Section 9.2.

7.1. PHYSICOCHEMICAL DESCRIPTION

Most models include a single species of dust. In rare instances, two differing species [17, 18, 21, 22, 23] or three [15] species have been incorporated in attempts to construct a model that can consistently represent the dynamical and optical properties of the dust. By "species," one has to understand either a more or less well-defined mineral (e.g., magnetite [57, 58, 59, 60], amorphous olivine [18, 22], amorphous carbon [18, 22]) or

“exotic dust” having “effective” physical properties (e.g., a small specific mass [30]): this, in some sense, allows for the fact that spinning grains with complex structures and shapes may be represented by spherical grains, but with “effective” properties differing from bulk material [18].

7.2. OPTICAL PROPERTIES

A model for the optical properties of the grains is needed to compute the grain temperature (equation 10), to compute the coma radiation field, and eventually to fit observed visible and IR emissions from the dust [18, 19]. In the last two cases, realistic optical constants of the selected materials must be used. Authors interested only in the temperature often use effective grain albedo and emissivity, defined by:

$$(1 - A_V^k) \int_0^\infty F_\lambda d\lambda \equiv \int_0^\infty F_\lambda Q_A^k(a_d, \lambda) d\lambda \equiv \dot{E}_{abs}(a_d, r) / \pi a_d^2 \tag{16}$$

$$\epsilon_{IR}^k \sigma_B [T_d^k]^4 \equiv \pi \int_0^\infty Q_A^k(a_d, \lambda) B_\lambda(T_d^k) d\lambda \equiv \dot{E}_{rad}(a_d, T_d^k) / 4\pi a_d^2 \tag{17}$$

However, it should be noted that the effective A_V^k thus defined is a strong function of the grain size (and a weak function of grain position at very low altitudes), and that the effective ϵ_{IR}^k is a strong function of both size and temperature (and a weak function of position). The use of constant values for A_V and ϵ_{IR} amounts, in fact, to prescribing the grain temperature and size: strong conclusions drawn from models making such an assumption are inappropriate.

7.3. SIZE DISTRIBUTION

In situ dust analysis performed during the Halley flyby missions [55, 61] has revealed a very broad dust mass spectrum, covering at least the range of 10^{-17} to 10^{-3} g. To allow for this fact, models use the “discrete approximation” by which the dust is represented by a certain number of single-size elementary fluids.

Only two works have used a representative large number of size classes (28 in [29], and 43 in [19, 22]). Figure 3 presents the variation with altitude and grain mass of the temperature and velocity of a distribution of amorphous carbon grains with a mass spectrum similar to that measured in situ in Comet Halley. One sees that the grains are nowhere in thermal equilibrium with the gas, and that the freespace temperatures and most terminal velocities are reached within a few kilometers from surface, even at large sizes. Notice, however, that small grains ($< 10^{-14}$ g) remain velocity-accommodated to the gas up to $\approx 10^3$ km from surface (at which altitude, they are uncoupled from it by the effect of solar radiation pressure!).

Most hydrodynamic models assume single-size dust (if any), and a few include a small number of sizes ([21, 23, 46, 47]). This raises the question: to what extent is a

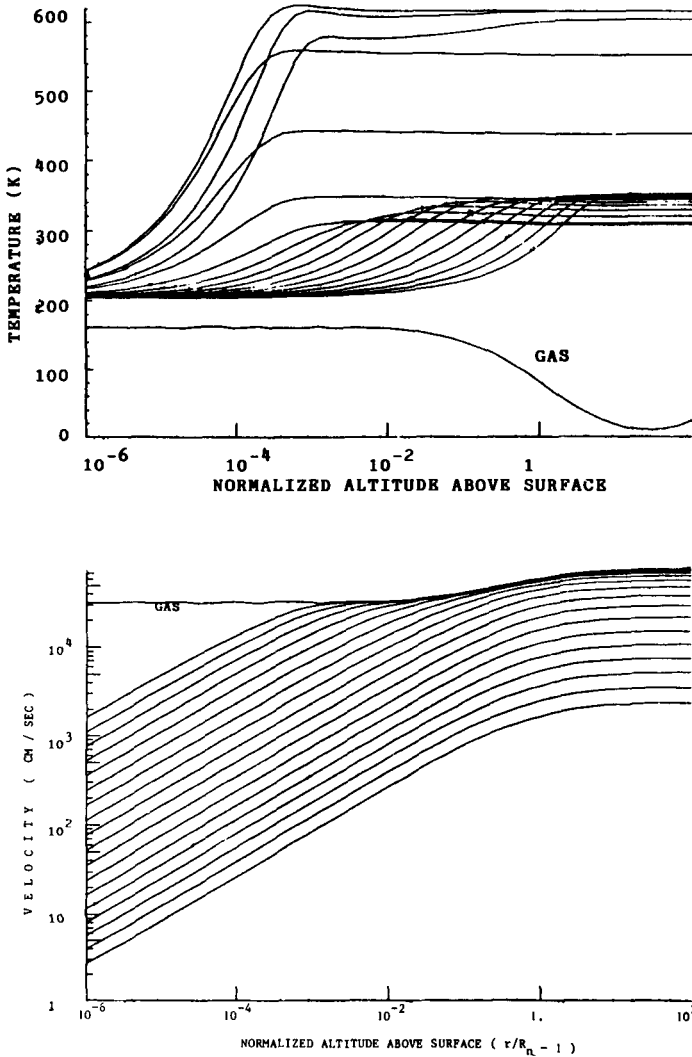


Figure 3. Relaxation of Comet Halley dust [18]. The expansion of a mixture of water and of amorphous carbon grains with a density of $0.3 \text{ g}\cdot\text{cm}^{-3}$ and with the in situ measured size distribution [55, 61] is computed. Dusty ice sublimation boundary conditions are assumed. The grain temperature and velocity are shown as a function of the normalized altitude above surface. The curves relative to dust are equispaced by factors of 10 in mass from 10^{-17} g to 1 g. Notice that grain velocity decreases monotonically with mass, but not grain temperature.

model that incorporates only a few dust classes suitable for representing the gas outflow? There is no universal answer to such a question. However, in the case of the in situ measured Halley dust distribution (as described in the interim assessment [55]), it has been shown, using the results of an hydrodynamic model incorporating 44 different grain mass intervals [22], that:

1. It is not correct to block the whole dust production rate into a small number of grain sizes—above all, of small grain sizes. As shown in many studies [66, 80], this approximation results in a strong perturbation of the gas by the dust. The real interaction is much smaller, because, in reality, a fraction of the mass is in the form of larger grains. The Halley distribution indeed results in very modest perturbations of the gas parameters.
2. It is possible to represent the dust distribution adequately (from the point of view of the interaction with the gas) by a small number of sizes, provided that the “effective sizes” and “effective mass loss rates” are selected very carefully: a mixture of single-size olivine grains and single-size amorphous carbon grains, with radii of 9 μm and a mass loss rate of only 5% olivine grains and 5% carbon grains relative to the gas loss rate, correctly achieves that purpose.
3. The sonic transition of the flow occurs within the first few meters from the nucleus surface.
4. This simple representation can by no means be used to adequately represent the optical properties of the dust distribution.

7.4. NONSPHERICAL GRAINS

Spherical grains have a minimal area-to-mass ratio. It can therefore be expected that nonspherical grains can be more easily dragged away. At small sizes, this is of little consequence, because even spherical grains assume terminal velocities practically identical to the low-altitude velocity of the gas [31, 62, 66]. It has been argued recently [32] that the effect of nonsphericity could be significant at large sizes, with, e.g., particles as heavy as a gram being capable of assuming a wide range of ejection velocities up to nearly that of the very small grains. Unquestionably, this effect must be taken into account when considering the formation of the dust tails and when evaluating the possible loss rates from a nucleus.

7.5. ICY GRAINS AND WATER CLUSTERS

If (dirty) ice grains are emitted from the nucleus, their sublimation will release water vapor (and other primary molecules and dust) [15, 80]. Here, however, the icy grains first act as sinks for the gas, after which, at higher altitudes, they start to sublimate [15]. Similarly, the small clusters, formed by homogeneous (and possibly ion-induced) recondensation, act as condensation centers up to a certain altitude, above which they are sublimated [17, 21, 44].

The treatment of these effects requires incorporation into the dust equations of specific terms allowing for the creation and annihilation of grains and for the evolution of the grain size. Also, the dust energy budget equation must incorporate terms representing the

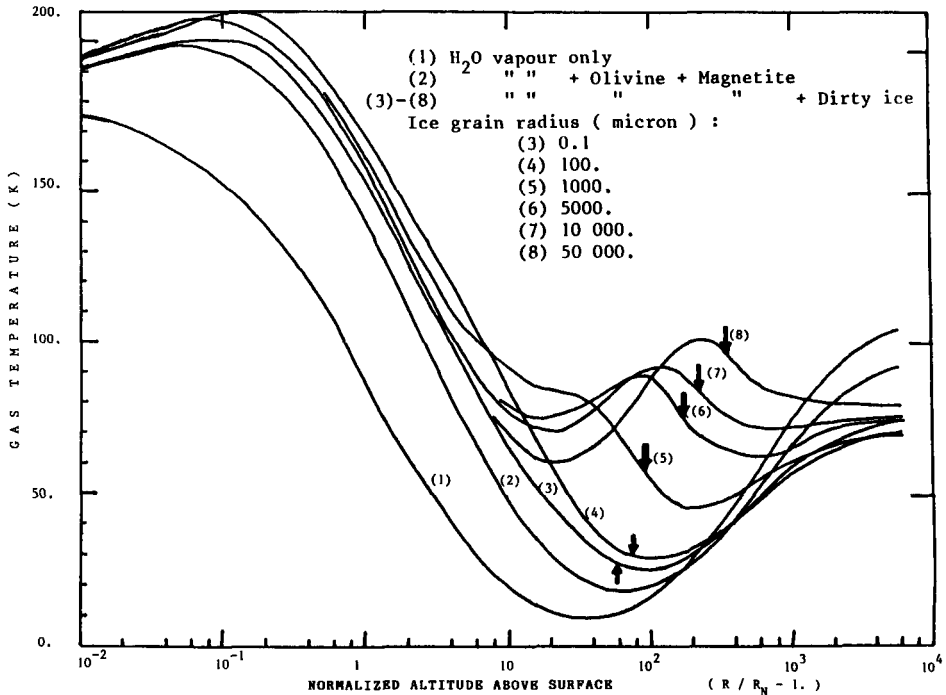


Figure 4. Hydrodynamic model of a dusty water coma with 30% of the water produced in a single-size icy grain halo. Various grain sizes are assumed. The arrows show the maximum distance reached by the grains. This distance is much smaller than the distance reached by water clusters, because the icy grains are assumed here to be dirty. From [15].

release and absorption of binding energy. Finally, the gas equations must incorporate specific terms representing the mass exchange and its implied momentum and energy transfers.

The case of icy grains (and clusters) has been exactly treated [15, 17, 21, 44], using free-molecular theory both for the momentum and energy exchanges and for the mass exchange (free-molecular sublimation and condensation). One of the essential results is that the water temperature is profoundly affected by the presence of icy grains and/or clusters. A typical result is shown in Figure 4. The effect is, however, limited to the survival zone of these grains and clusters, i.e., the innermost coma (within ≈ 1000 km at a 1-AU heliocentric distance).

7.6. ACTIVE DUST

The observation of brightness patterns (loosely called "jets") in the emission of some minor molecules (e.g., CN and C₂ [11]) and of unexpected low-altitude brightening of dust jets [75, 77] has suggested that the dust released from the nucleus could undergo

reprocessing in the coma. One of the possible sources of dust “activity” is the fast heating up of the grains (if they are emitted from cold icy surfaces): pyrolysis [81] and fragmentation [42, 77] are, in this case, possible.

The case of fragmentation or outgassing of refractory grains has been subject only to heuristic treatments [11, 42, 81]. One of the difficulties is that the problem must be approached under nonspherical geometry if jet-like patterns are to be obtained. Besides this, water and outgassed minor molecules must be treated as two separate fluids, since their spatial distributions need to be distinct. Models incorporating two distinct neutral gas species have not been developed, even in spherical geometry. Appropriate gas-dynamic methods exist, but their adaptation to the present problem may not be trivial.

7.7. VERY LARGE GRAINS

The maximum size of spherical grains that can be ejected from a nucleus has been estimated from setting $\underline{V}_i = 0$ in equation (2) applied to the dust, i.e., from balancing the drag force by the nucleus gravitational force (e.g., [31, 80]). However, one then currently gets grain radii much greater than the water free path at the surface [17]. Accordingly, the free molecular expression for the drag is not usable. Figure 5 compares the currently accepted (free molecular) values with more realistic estimates based on transition regime drag coefficients [19]. Error bars indicate the estimated dispersion associated with nonspherical shapes. These results apply to a spherical nucleus. In reality, the maximum liftable mass will also depend upon the position on the nucleus.

Even if lifted from the nucleus surface, a large grain does not necessarily escape from the immediate vicinity of the nucleus. It may eventually fall back onto the surface or escape very slowly via spiralling orbits or even stay in a trapped near-nucleus orbit [4]. This, for instance, complicates the interpretation of information (e.g., radar echoes, and in situ impacts) received from heavy grains in the central region of comets [9].

8. Photochemical Budget

The main purpose of introducing a network of chemical rate equations in comet models is, of course, to account for the consumption of parent molecules and for the formation of daughter species. Here, we are concerned only with the net mass, momentum, and energy budget of these processes. Formally speaking, when the daughter species are grouped with the parent molecules into a single fluid, these budgets are represented by the terms \underline{P}_{ij} and \underline{E}_{ij} , but if some daughter products are separated into daughter fluids (e.g., ions, [51, 57] or atomic hydrogen [36, 58]) or treated by a Monte Carlo method [7, 12, 13], the exchanges are represented by terms \underline{M}_{ij} , \underline{P}_{ij} and \underline{E}_{ij} .

8.1. MOMENTUM BUDGET

The momentum budget has been evaluated by only a few authors [35, 36, 69]. Results have been presented only for a 1-AU heliocentric distance [35] and indicate a momentum loss at low altitudes (10^3 to 10^4 km), followed by a momentum gain. But the magnitude of the effect is small. It is due essentially to exchanges with atomic hydrogen. Most models omit this term.

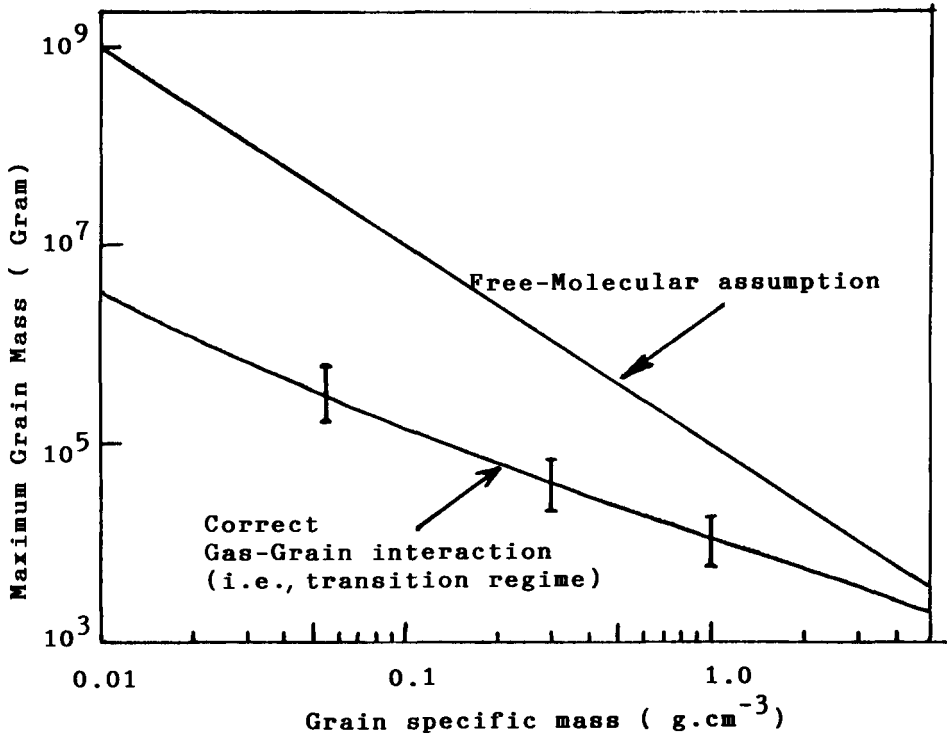


Figure 5. The maximum mass of a grain that can be lifted from Comet Halley at flyby conditions as a function of assumed grain specific mass [18, 19]. The comet nucleus is assumed to be spherical. The curve labeled "free-molecular" is obtained by assuming spherical grains with drag coefficients given by free-molecular formulas. The curve labeled "correct" assumes spherical grains with realistic drag coefficients. The error bars indicates plausible dispersions introduced by nonsphericity of the grains.

8.2. ENERGY BUDGET

A term representing the energy budget is included in almost all models; it has been recognized that this effect is due dominantly to collisions with the energetic dissociation products of H_2O , mostly H and OH, and that it controls the water temperature and velocity in the outer coma.

We can formally write the rate of energy deposition from photochemical processes as:

$$\dot{E}_{\text{ch}} \text{ (erg s}^{-1} \text{ molecule}^{-1}\text{)} = \sum \beta(r) \Delta E \alpha_1 \alpha_2(r) \quad (18)$$

where $\beta(r)$ is the local H_2O dissociation rate (altered by coma absorption at very low altitudes, and dependent upon solar activity), ΔE the dissociation energy excess, α_1 the fraction of ΔE that is under the form of fragment kinetic energy, and $\alpha_2(r)$ the fraction of ($\alpha_1 \Delta E$) that is transferred locally (i.e., within a few m.f.p.) to H_2O by collisions. The sum is to be performed on each of the possible dissociation branches (85% is in the branch $\text{H}_2\text{O} \rightarrow \text{OH} + \text{H}$).

There is general agreement among authors with respect to $\beta(\infty)$ given by [25]:

$$\beta(\infty) = 1.26 \times 10^{-5} [1 + 0.0032 (F_{11} - 65)] \text{ s}^{-1} \quad (19)$$

in which F_{11} is the 10.7-cm flux from the Sun (in janskys). (For solar minimum, $F_{11} = 65 \text{ Jy}$.)

There is considerable confusion with respect to the other terms, unfortunately. From a critical analysis based on recent laboratory data [25], the following values can be recommended for ΔE and α_1 in the main dissociation branch at 1 AU from the Sun:

$$\Delta E = 3.4 \text{ eV} \quad \alpha_1 = 0.54 \quad (20)$$

This combination is beginning to be adopted [12, 23, 33]. However, the works published between 1985 and 1986 often use the value $\alpha_1 = 1$, which ignores the fact that part of the dissociation energy is lost via radiative de-excitation of the OH radical [13, 15, 17, 21, 24, 31, 35, 40, 69]. Earlier works assume both incorrect values for ΔE (taken to be equal to 1.9 eV) and for α_1 (taken to be equal to 1), but, by mere coincidence, the product $\alpha_1 \Delta E$ turns out to be nearly correct [36, 57, 58, 59, 60, 61, 62]!

While reliable values seem now at hand for β , ΔE , and α_1 [25], such is not the case for the function $\alpha_2(r)$. This function is smaller than unity in most of the outer coma because the fast dissociation fragments (mostly fast H) have a thermalization free path much greater than the local H_2O free path. A certain number of works ignore this fact and take $\alpha_2 = 1$ everywhere [30, 31, 49, 50, 78]. A few others ignore the whole effect itself (i.e., assume $\alpha_2 \equiv 0$) [44]. However, most works incorporate a position-dependent function $\alpha_2(r)$. Various methods have been proposed to derive this function:

1. Heuristic analytic expressions [7, 38, 43].
2. Monte Carlo simulation of the interaction of the dissociation fragments with water [7, 12, 13, 40], not to be confused with DMC simulation of the coma [33].
3. Radiation transfer approximation for this interaction [35, 36, 37, 69].
4. Incorporation of H into a multifluid model under the form of a "normal" hydrogen fluid, plus a zero-temperature fast "prethermal" fluid [57, 58, 59, 60, 61, 62].

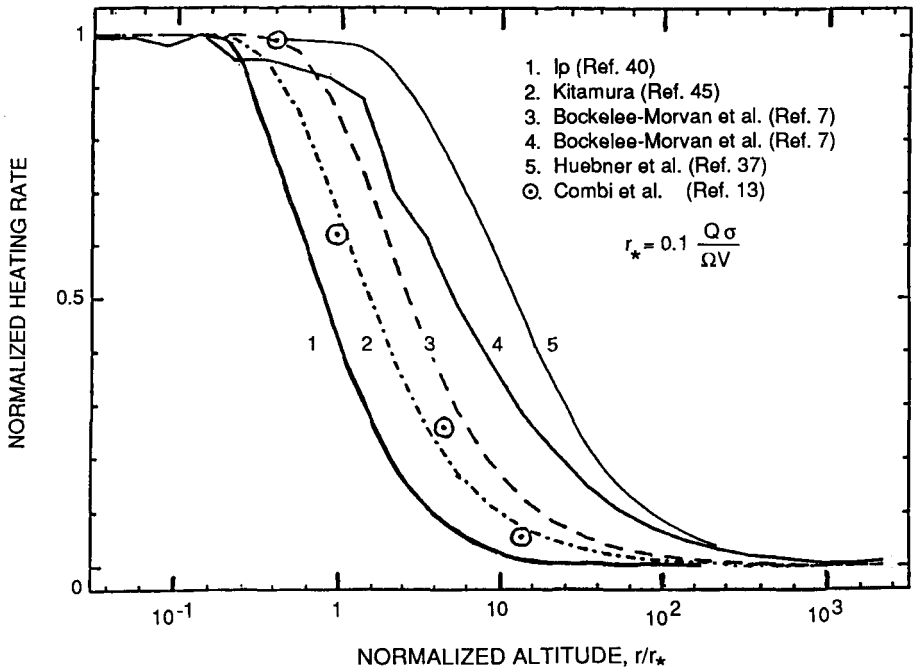


Figure 6. The photochemical deposition profile $\alpha_2(r)$ computed by various authors. For Comet Halley flyby conditions, r_* is about 5000 km. Notice that this function critically controls the water temperature and outflow velocity above r_* .

Figure 6 compares the function $\alpha_2(r)$ obtained by some of these methods. It is seen that:

1. Those models interested only in the properties of the innermost coma can use the approximation $\alpha_2 \equiv 1$ [29, 30, 45, 46, 47, 52].
2. Qualitatively, the shapes of $\alpha_2(r)$ obtained by various authors agree.
3. Quantitatively, these forms disagree.
4. It is certainly unacceptable to use $\alpha_2 \equiv 1$ far out in the coma.

One way of discriminating amongst the differing functions α_2 would be to extract α_2 from a “full” Monte Carlo simulation [33]. Unfortunately, at this time, this has not yet been done.

9. Radiative Effects

The basis for a discussion of radiative effects is the rate equation (8). In a binary encounter, a molecule can lose kinetic energy by exciting internal modes of its partner, or it can gain kinetic energy by de-exciting these modes (quenching). The net budget depends upon the level population distribution P_j . The latter itself depends on these collisions, on the level lifetimes, and on the interaction with the radiation field (absorption and stimulated emission). Kinetic energy can therefore be exchanged with the radiation field (heating or cooling). For the water molecule, these effects occur at infrared wavelengths. The ultimate sources of possible radiative energy inputs into the molecule are the sources of the IR radiation field, i.e., the Sun, the coma dust, and the nucleus.

The net momentum budget (radiation pressure) of these effects is neglected by all authors. This is probably justified in view of the fact that the radiation pressure on species that fluoresce in the visible is ineffective in the inner coma [62] and that the IR radiation density is much smaller than the visible light one.

It is important to realize that, in equation (3), the term \dot{E}_r , which allows for the radiative energy exchanges, must represent the rate of energy exchange between the local radiation field and the local fluid element (with a typical volume \approx the cube of m.f.p.), not between the local radiation field and a single molecule: photons with a m.f.p. smaller than the local gas m.f.p. do not contribute. Also \dot{E}_r should not be confused with the coma radiative budget, i.e., photons with free path greater than the local gas m.f.p., but smaller than the size of the coma, do contribute.

9.1. RADIATIVE BUDGET OF THE WATER MOLECULE, IGNORING THE DUST AND NUCLEUS RADIATION

This problem has been solved consistently with radiative transfer computations in the rotation and vibration bands [6, 7, 23, 24]. Unfortunately, analytic expressions approximating these results have not yet appeared.

The definition of \dot{E}_r must be done carefully. In the innermost coma (within 1000 km at 1 AU from the Sun), LTE prevails among the rotational levels of water. It is then possible to precisely define a function $\gamma(T)$ [24] to be inserted in equation (6), and \dot{E}_r will then assume the form of a function $L(T, Q_{\text{eff}})$, with Q_{eff} being the effective spherical production rate (see Section 12.2). However, at higher altitudes, the rotational populations are nonthermal. Therefore, it is more sensible to take $\gamma \equiv 5/3$ (full relaxation), and \dot{E}_r will then assume another form $\Lambda(T, r)$ [7]. Of course, in the innermost coma, either one of these representations can be used, and there is a simple relation (there only) between L and Λ [20]. For the results presented here, we arbitrarily adopt the "L" definition throughout the coma. Figure 7 shows an example of a radiative term (in the "L" definition) computed in a model that consistently incorporates water excitation, multicomponent dust, and water recondensation, with numerical values appropriate for Halley flyby conditions [23]. One sees that radiative effects are negligible in the innermost coma with respect to the dust heating and to the water recondensation heating. The opposite is true in the outer coma (i.e., throughout the observable coma), where radiative cooling is of the same order of magnitude as photodissociative heating. Indeed, preliminary investigation reveals that this is probably not circumstantial: rotational cooling operates as a feedback mechanism that

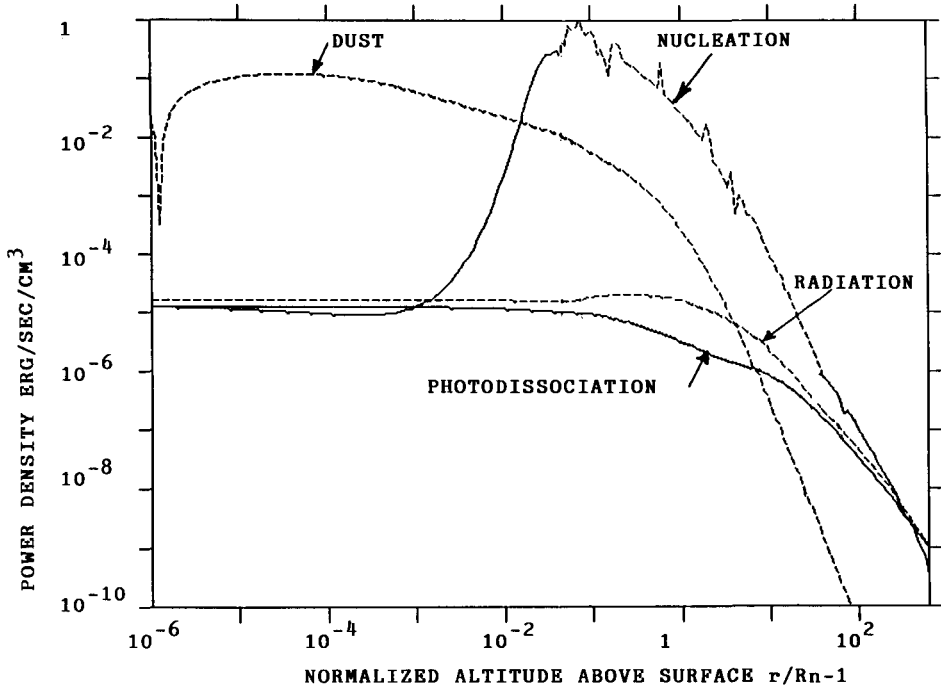


Figure 7. Energy exchange terms entering into the gas energy equation under Comet Halley flyby conditions [23]. The model incorporates polydispersed dust representative of Halley flyby results [55, 61], water recondensation [21] and water radiative losses computed from a realistic excitation model [6]. Photochemical heating is approximated by an analytic expression [7]. **WARNING:** These terms are highly nonlinear versus gas production rate and should not be scaled for other conditions.

buffers the water temperature. If this is confirmed, it will place less severe demands on the accuracy of the evaluation of the photochemical heating source!

Attempts at bypassing the exact treatment by using an heuristic expression \dot{E}_r have resulted in a wealth of equally improper expressions:

1. An approximative expression for the individual molecule cooling rate originally proposed in [71] is still being used by some authors [30, 38, 45, 46, 47, 58, 78].
2. Other authors multiply this term by a coma optical thickness factor, thereby making an overcorrection [12, 13, 31, 35, 36].
3. Others simply omit the term [15, 16, 17, 18, 19, 21, 22, 52].
4. Others conservatively present two solutions, one with the molecular cooling of reference [71] and the other with no term at all [39, 40, 49, 50].

5. Finally, the full comprehensive treatment is incorporated in [6, 7, 23, 24].

9.2. THE EFFECT OF THE NUCLEUS AND DUST THERMAL EMISSION

In a simplified treatment of the coma radiation field already mentioned [60], it was found that the dust emission could very efficiently heat the innermost water coma. A semi-empirical algebraic expression was proposed and later on used by some authors [29, 31]. However, this result was challenged by simple estimates based on a simple representation of the dust (and nucleus) radiation fields and taking into account the detailed excitation of the water molecule [6, 7]. The original work [60] was recently reconsidered [57], with results indeed much smaller than originally evaluated. A precise numerical estimate is, however, not available at this time.

10. Water Recondensation

10.1. HOMOGENEOUS RECONDENSATION

As already mentioned, water vapor becomes quickly unstable with respect to recondensation, due to the fast increase with altitude of the supersaturation ratio:

$$S = p/p_s(T_g) \tag{21}$$

with $p_s(T_g)$ being the water sublimation pressure [16, 17, 21, 39, 44].

Two distinct populations of water clusters $(H_2O)_j$ are formed:

1. The so called “subcritical” clusters, with $2 < j < j_*$, where j_* is a certain “critical size” function of S and T_g . The concentration of these clusters decreases rapidly with increasing j ; thus, only the dimer is important. Typical dimer mole fractions are in the range of 10^{-2} to 10^{-5} under Halley flyby conditions [21].
2. The “supercritical” clusters are formed in a catastrophic process. After their “creation,” these clusters evolve as pure icy grains, i.e., they grow by water condensation until solar illumination and gas dilution reverse the trend, making the clusters shrink and disappear. The rate of appearance of supercritical clusters is given in the “Modified Becker Döring” approximation [21] by:

$$J \equiv \underline{V}_c (n_c \underline{V}_c) = \frac{n_g^2}{\rho_c S} \sqrt{\frac{2\sigma_c m_g}{\pi}} \exp \left[\psi - \frac{4\psi^3}{27(\ln S)^2} \right] \tag{22}$$

with

$$\psi = (36 \pi m_g^2 / \rho_c^2)^{1/3} \sigma_c / kT_g \tag{23}$$

and with n_c and \underline{V}_c being the cluster number density and flow velocity (initially equal to \underline{V}_g), σ_c and ρ_c the ice surface tension and specific mass, and m_g , n_g , and T_g the water molecule mass, number density, and temperature.

The cluster initial size j_* is given by:

$$j_* = [2\psi/(3\ln S)]^3 \quad (24)$$

By using any existing coma water density and temperature profile, it is trivial to verify the following facts (see also Figure 8):

1. J peaks in a very narrow altitude range (typically ≈ 100 m!) near the nucleus surface, but well inside the supersonic region of the expansion.
2. In this region, j_* is on the order of 10 molecules/cluster.

Therefore, one can use the "sudden onset" or "catastrophic" approximation [17, 21, 44] that all clusters are produced at the altitude where J peaks. Subsequently, they all evolve at higher altitude in the same way, i.e., they form a fluid with no size dispersion

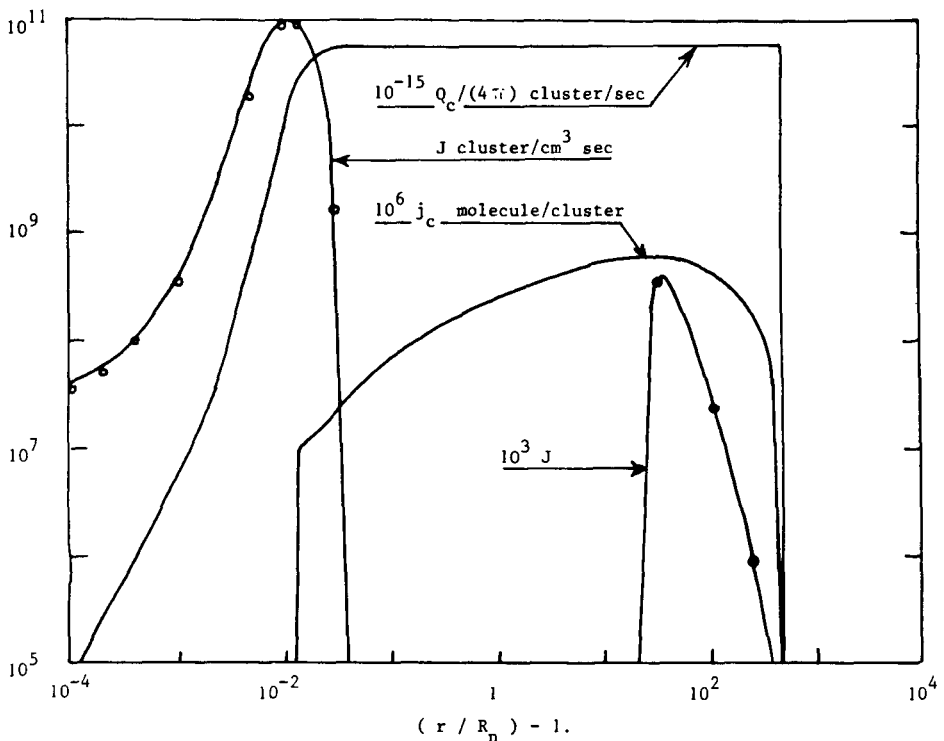


Figure 8. Predicted water homogeneous recondensation under Halley flyby conditions [21]. J is the rate of cluster production, Q_c the cluster flux, and j_c the number of molecule per cluster. The secondary peak in J is real, but does not have significant effects.

(but with altitude-dependent size). The production rate of this fluid can be computed by integration of (18) in the vicinity of the peak:

$$Q_c = \int J dr / V_g \quad (25)$$

Model predictions appropriate for P/Halley flyby conditions are shown in Figure 8. All studies [17, 21, 39, 44] agree that, near a 1-AU heliocentric distance, the fraction of water recondensed is at most 15%, and the cluster range is at most 1000 km. The main effect of the process is to considerably heat the gas, as icy grains would do, and accordingly to increase its outflow velocity. This is expressed in the gas equations by terms E_c and P_c that are similar in form to those appropriate for icy grains (Section 7.5). The recondensation energy source is, in fact, dominant in the first thousand kilometers, at least under Halley flyby conditions (Figure 7).

The predictions of the homogeneous nucleation theory can be shown to be contingent upon the efficiency of formation of the water dimer by binary collisions. This efficiency has, at the present time, not been measured. Therefore, one cannot exclude the possibility that the present predictions overestimate the effect, even though this is not likely [21].

Finally, let us point out that the catastrophic recondensation, as computed in [21], is just barely “subcritical” (in the gas dynamic sense), i.e., the heating of the gas is not strong enough to induce the formation of a standing shock. For slightly higher water production rates, one expects such a shock to occur (as observed in moist supersonic wind tunnels) with associated flow divergence (under nonspherical conditions). This remains to be studied in the future.

10.2. HETEROGENEOUS RECONDENSATION

In Nature, a supersaturated vapor often recondenses easier via heterogeneous processes than via the homogeneous route. Heterogeneous recondensation in a cometary coma can take place on dust grains or on ions.

In the modeling of the hydrodynamic interactions between cometary gas and dust, it is assumed that all water molecules impacting on a grain are reemitted. However, if the grain temperature is below the triple point of water T_p (0.01°C), current experience indicates that water can adhere efficiently to the surface, forming frost. Inspection of Figure 3 reveals that the small grains, which offer the maximum cross-section for the gas, are heated very fast to well above T_p . Therefore, although no quantitative modeling of water recondensation on dust has yet appeared, it seems likely that this effect is negligible [21, 44].

Recondensation of water on ions is a very efficient process in, for instance, the terrestrial ionosphere (D region). The similarity in temperature between P/Halley’s coma and the D region suggests that this recondensation process may occur also in a coma [21, 62]. As an original contribution to this study, we have developed a chemical model of a pure water coma, in which both homogeneous and ion recondensation are incorporated. A detailed account of this model will be presented elsewhere. Figure 9 shows an example of results. One sees that the peak ion density region is dominated not only by H_3O^+ , as previously predicted, but by the complete family of ions of the kind $H^+ (H_2O)_j$. Also, in the

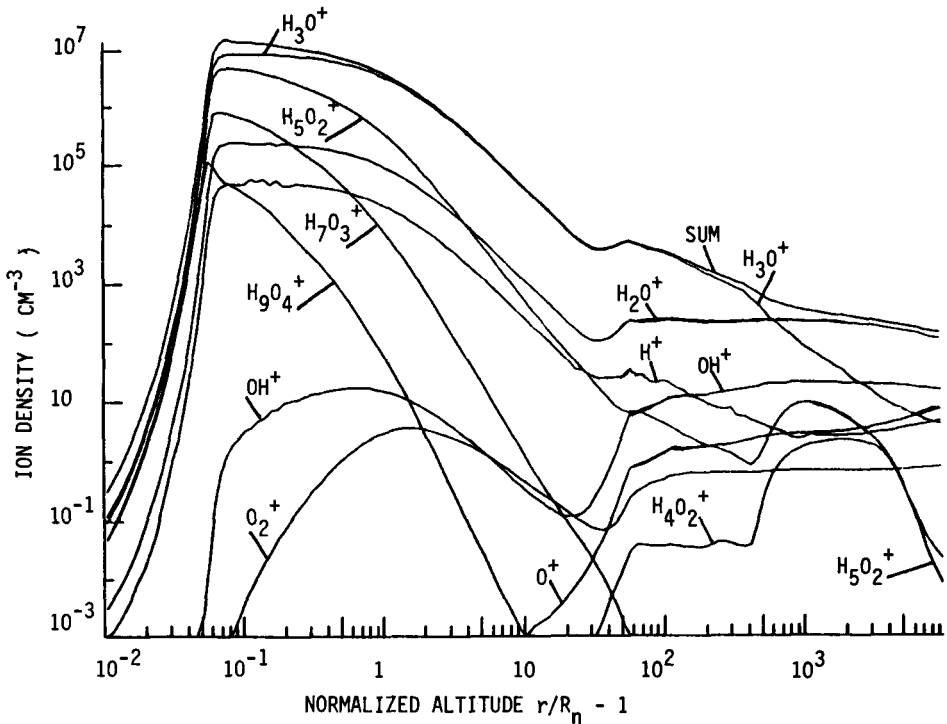


Figure 9. Predicted ion composition of a pure water coma under Comet Halley flyby conditions, taking into account homogeneous and ion recondensation. Notice the dominance of heavy water group ions near the ion density peak, and a secondary peak in heavy ion density associated with the coma temperature minimum (near $10^3 R_n$).

region of minimum coma temperature, a significant abundance of these ions and of those of the family $(H_2O)_j^+$ is predicted. As far as charged supercritical clusters are concerned (large j), realistic computations of J are not possible for want of appropriate physical parameter values. However, since the concentration of charged subcritical clusters is at least two orders of magnitude below that of neutral subcritical clusters, the same relative concentration will probably be true for the abundances of charged and neutral supercritical clusters.

11. Electrons and Ions

The collisional coma is a weakly ionized medium, even though it is almost everywhere transparent to the ionizing solar light. Close to the comet, the water group ions (H_3O^+ , H_2O^+ , OH^+) were found to be predominant (as predicted) by the in situ instru-

ments. The ratio n_i/n_g is about 10^{-2} at an altitude of 10^4 km. The reason for this small value is essentially that the atmosphere here is in expansion, not in a hydrostatic state (i.e., the flow time is smaller than the ionization time).

The success of (magneto)hydrodynamic equations (MHDEs) in modeling even extremely tenuous ionized media (e.g., the solar wind) is well-known. It seems that MHDEs can indeed account satisfactorily for most observed properties of the cometary plasma (e.g., [14, 69, 83, 84]). Here, we will discuss only the innermost region of the coma, the so-called “diamagnetic cavity” (DC), where, as revealed by the Giotto mission magnetometer, the magnetic field is negligibly small (less than 0.1 nT). In such a case, the MHDEs reduce to the NSEs. The formation of this cavity is well-understood [83, 84]; its shape is predicted to depend upon the pattern of neutral gas production, and its size upon the absolute value of the gas production rate. Its boundary was crossed by the Giotto spacecraft near an altitude of 4000 km.

At the most primitive level of modeling, electrons and ions are assumed to be fully accommodated to the neutral gas and only number densities are computed by chemical rate equations of the form (9) ([1, 35, 36, 47] and Figure 9 of this study). Other authors use a separate electron fluid, but keep the ions inside the neutral fluid [58, 59, 60, 69, 83]. In a few studies, both ions and electrons are treated as separate fluids [14, 51, 57]. In fact, the lumpings of all ions in a single fluid and of all electrons in a single fluid raise difficulties as we will comment below [51]. For the sake of brevity, we will only give a brief overview of the structure of the governing equations presently in use, to outline differences and similarities with those of the neutral gas.

11.1. ELECTRIC CHARGE BUDGET

It is convenient to use charge instead of mass, since the plasma neutrality requirement implies $n_i \equiv n_e \equiv n_p$. The governing equation for n_i , with equation (1), expresses the balance between (photo)chemical production and recombination loss. Since $n_g \gg n_p$, the former has an approximate r^{-2} dependence, and the latter is proportional to n_p^2 . Thus, if the flow time does not exceed the chemical time, one expects n_p to exhibit an r^{-1} dependence [14]. This is approximately verified above the initial fast n_p increase region (see Figure 9 and quoted references) up to the vicinity of the DC boundary, where additional processes come into play.

11.2. MOMENTUM EQUATION

The equality $n_e = n_i$ requires a common flow velocity V_p . When there is no separate ion fluid, $V_p \equiv V_g$. Otherwise, the inviscid equation (2) is used for V_p [51] or the exact NSE ([14], but notice that the Cartesian form of the viscous term is written there in lieu of the spherical form). In spherical geometry, one has:

$$\frac{1}{r^2} \frac{d}{dr} (r^2 \rho_j V_p^2) + \frac{d}{dr} \left(\rho_j \frac{k_B T_j}{m_j} \right) - \frac{4}{3} \mu_j \frac{d}{dr} \left(\frac{dV_p}{dr} + 2 \frac{dV_p}{dr} \right) = \dot{P}_{jn} + F_j + \dot{M}_{jn} V_g - \dot{M}_{ic} V_p \tag{26}$$

in which j labels electrons or ions, \dot{M}_{jn} is the photoproduction source, \dot{M}_{ie} is the recombination sink, and μ_j is the shear viscosity. There is no \dot{P}_{jj} term (equation 2) to the extent that electrons and ions are produced isotropically, P_{jn} is a drag force resulting from the collisions with neutrals, and the body force \underline{F} is the force $\pm en_p \underline{E}$ due to the polarization electric field \underline{E} , which maintains charge neutrality. We come out with two unknowns, V_p and \underline{E} , for which two equations are available (the ion and electron momentum budget).

11.3. ENERGY EQUATION

As is the case for neutrals, the construction of relevant energy equations for ions and, above all, for electrons raises many difficulties. An inviscid equation of the form (3) is used in [69] for electrons; an intermediate equation (NSE, but with the viscous dissipation term omitted) is used for electrons in [57, 58, 59, 60] and for ions and electrons in [14, 51]. Using, e.g., equation (12) of [20], we can write this energy equation:

$$\frac{1}{r^2} \frac{d}{dr} \left\{ r^2 \left[\rho V_p \left(\frac{1}{2} V_p^2 + \frac{\gamma}{\gamma-1} \frac{k_B T}{m} \right) \right] - k_c \frac{dT}{dr} \right\} + \frac{4}{3} \mu \left[\frac{V_p}{r} \frac{dV_p}{dr} - \left(\frac{dV_p}{dr} \right)^2 \right] = \quad (27)$$

$$\Sigma \dot{M} \left(\frac{V_p^2}{2} + \frac{3}{2} k_B \frac{T}{m} \right) + \dot{E}_{rad} + \dot{E}_{chem} + \dot{E}_{n,el} + \dot{E}_{n,incl} + \dot{E}_{ch,el} + (\dot{P}_n + F) V_p$$

where the sum extends over the \dot{M} defined in (26), the \dot{E} will be discussed below, and k_c is the heat conductivity coefficient. In the case of pure Coulomb interactions [20]:

$$\mu = (5/2) C (1) T^2 \sqrt{mk_B T} ; k_c = (15/4 + d_i) (k_B/m) \mu \quad (28)$$

with d_i being the number of active internal degrees of freedom, and $C(1)$ being a constant defined, e.g., in [20].

Owing to the dependence upon mass of μ and of k_c , the viscous dissipation is expected to be more important for ions than for electrons (however, at this time, it is not considered in cometary models), and the heat conduction term is expected to be more important for electrons. The simple expressions of (28) must be modified whenever significant particle momentum transfers are induced by processes other than ion-ion or electron-electron collisions. Restricting the discussion to the electron thermal conductivity, a proper expression must allow for the following effects:

1. Existence of the polarization electric field, which opposes the electron motion in the direction of the temperature gradient.
2. Competition between ion-electron and electron-electron collisions.
3. Competition between electron-neutral and electron-electron collisions.

The outcome is an heuristic expressions of the form:

$$k_c = a_1 T^{5/2} / (1 + a_2 T^{a_3} \rho_g / \rho_e) \quad (29)$$

but the values adopted for a_1 , a_2 and a_3 vary from author to author [14, 51, 57, 58, 59, 60]. Besides this, as noted in [51], even a residual magnetic field below the sensitivity level of the Giotto magnetometer, if present in the DC, could considerably reduce the electron conductivity, making a realistic evaluation of this term quite uncertain.

\dot{E}_{rad} is the radiative exchange term, nonexistent for electrons, but not necessarily so for polyatomic ions, which can be produced in excited states and collisionally excited or quenched. Existing models do not consider these effects presently, with the exception of [57], in which IR exchanges are represented by heuristic expressions inspired from those used for H_2O .

\dot{E}_{chem} represents the energy input due to chemical processes. For ions, it is predominantly due to excess energy released in ion-molecule reactions (i.e., mostly ion- H_2O), which is assumed to be locally redistributed among ions (rather than shared between ions and neutrals). Furthermore, the questionable assumption that light ions (e.g., H^+) share a common temperature with the heavy ones is made. For electrons, \dot{E}_{chem} is essentially due to the excess energy carried away by newborn photoelectrons. However, the magnitude of this excess (up to more than 50 eV) is such that local thermalization may not prevail. In many respects, this problem is similar to that arising for fast hydrogen atoms (Section 8.2). Most models presently assume local thermalization [57, 58, 59, 60, 69], but in one case, a two-stream method was used to improve the modeling [51]. It is likely that a satisfactory treatment will require more sophisticated methods, where a strongly non-Maxwellian shape will be allowed for the electron velocity d.f. This is required not only to obtain a proper energy budget of the plasma, but also to properly evaluate the chemical reactions in which only energetic electrons take part (secondary ionizations and dissociations), as well as the contribution of electrons to the excitation of various molecules, including water itself [7].

$\dot{E}_{n, \text{el}}$ and $\dot{E}_{n, \text{inel}}$ are, respectively, the rates of energy exchange with the neutral gas via elastic and via inelastic collisions. In view of the ratios of the masses involved, one may expect that $\dot{E}_{n, \text{inel}}$ will be dominant in the cases of electron-neutral collisions and $\dot{E}_{n, \text{el}}$ dominant in the case of ion-neutral collisions. In the former case, it is agreed that rotational and vibrational-electronic excitation of water is the dominant electron cooling process [14, 51, 58, 69]. (However, this does not imply that it plays an important role in the excitation of the water molecule itself [7].)

Finally, \dot{E}_{ch} is the rate of elastic Coulomb energy exchange between ions and electrons. Neglected in [58, 68], which do not have an ion energy equation, it is incorporated in [51].

11.4. PLASMA VELOCITY

Figure 10 shows an example of a computed inner coma plasma velocity field [51]. One can see that, as is the case for the neutral gas velocity, the results depend upon the assumptions made for the thermalization of the fast dissociation products (here, electrons). Aside from this, the key effect is the initial plasma deceleration—in fact, down to subsonic flow. It is mainly due to deceleration by the hot electron pressure resulting from the fast rise in electron temperature (see below). Beyond the velocity minimum, the model should be considered unrealistic, because effects associated with the formation of the DC boundary should be taken into account [14].

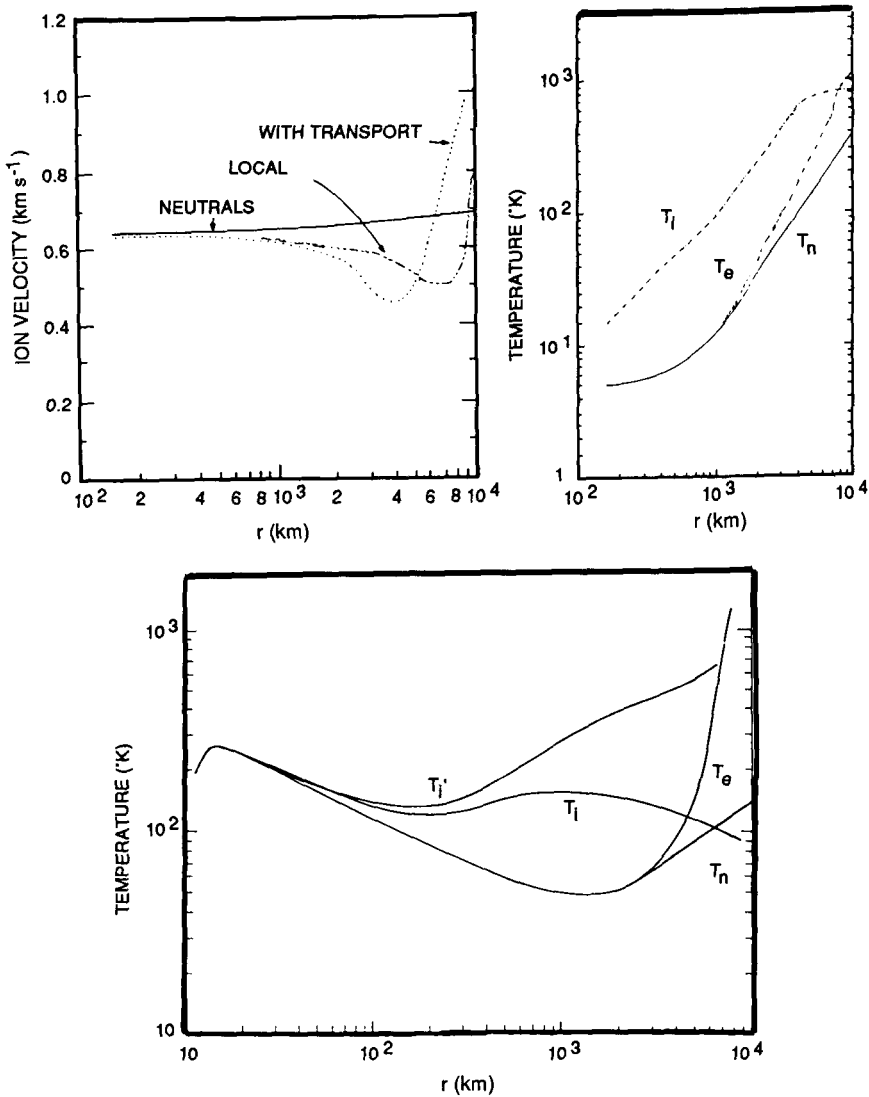


Figure 10. Model properties of inner coma ions and electrons under Comet Halley flyby conditions. The two upper panels are from [51] and the lower panel from [57]. The two ion velocity fields shown in the left upper panel are computed assuming local (...) or non-local (-.-) photoelectron thermalization. The two ion temperature fields in the lower panel are computed assuming (T_i) or neglecting (T_i') radiative ion cooling.

11.5. PLASMA TEMPERATURES

Figure 10 presents two independently computed temperature fields [51, 57]. One sees that the electron temperature is kept accommodated to the neutral temperature by inelastic collisions, until photochemical heating prevails. In contrast to this, the ion temperature quickly uncouples from the neutral one, under the effect of ion chemical heating. Notice that the neutral temperature in these models is obtained from rather primitive neutral gas equations, so that the computation of really convincing coma temperatures still remains the subject of future, more comprehensive models. In any case, the use of in situ measured ion temperatures to infer neutral gas temperatures [1] is certainly unwarranted.

12. Initial Boundary Conditions

In principle, understanding the boundary conditions that govern the outflow of coma material is the ultimate purpose of cometary modeling, since it will give access to a wealth of properties of the nucleus surface. It can be shown, for instance, that the reality of ice sublimation cannot be proven by remote sensing of the nucleus because the relevant temperature range (< 200 K) is not accessible to infrared sounding due to the masking effect of coma dust emissions [18]. Also, the boundary condition assessment is essential for the understanding of many (but not of all) coma processes. From the point of view of the coma, the initial boundary conditions are of two distinct kinds:

1. Structural properties of the nucleus, i.e., the shape of the surface on all scales, chemical composition on all scales, temperature on all scales, loss rates at each position, and so on.
2. Coma/nucleus interfacial properties. This subtle problem has been overlooked for a long time, although some relevant treatment had been offered in the case of icy sublimation [72]. The essential physical fact to be recognized is that due to the initial fast (nearly sonic) expansion, the gas is not in thermal equilibrium with the surface of the nucleus. Accordingly, the gas d.f. has a non-Maxwellian shape in a transition region (or “boundary layer” or “Knudsen layer”) adjacent to the surface. Methods based on the Boltzmann equation must be used to assess the initial gas parameters (see Section 12.5).

12.1. LESSONS FROM HALLEY FLYBY OBSERVATIONS

Common sense suggests that cometary nuclei, as with any small-size solar-system solid object, do not assume a simple shape. A rough approximation of the Comet Halley nucleus is an ellipsoid with dimensions of $4.1 \times 4.2 \times 8$ km; the low-altitude dust production pattern reveals a wealth of discrete emission areas, with most of the production occurring from three regions with estimated areas of 7, 7, and 22 km² (with the total nucleus area being estimated at 400 km²) [41]. On the other hand, the large-scale distribution of water reveals only moderate asphericity [82]. Furthermore, as shown in Figure 11, a spherically symmetric stationary solution of equation (1) for water, with \underline{Y} taken from the in situ measurements [53], fits the in situ measured water density well, even though the flyby trajectory spanned more than 90° in local solar zenith angle [1]. The inner coma gas transit times (a few hours) are much smaller than the nucleus rotation period, so rotational

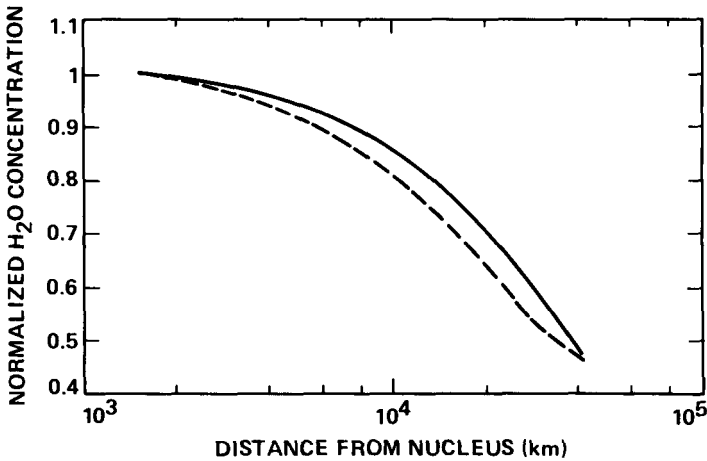


Figure 11. Giotto neutral mass spectrometer (NMS) results (solid line) and model values (dashed line) for H₂O normalized by the value at the smallest distance and scaled by r^2 to correct for spatial dilution from spherical outflow [1].

blur effect cannot be important. Explanation for this discrepancy is a challenge for coma models.

Numerically speaking:

1. The total gas production rate corresponding to the in situ measurements (acquired above 1500 km) is $\approx 4 \times 10^{29}$ molecules/s ($\pm 50\%$) if the outflow of water is spherically symmetric (over 4π steradian).
2. The minimum solar beam cross-section required for producing this outflow at 0.9 AU from the Sun is 19 km^2 ($\pm 50\%$), which is intermediate between the minimum and maximum nucleus cross-section. Therefore, there is no objection against production of gas from most of the sunlit part of the nucleus, but if it is so, then one must explain why dust production is restricted to small areas.
3. The dust-active areas are sufficient for obtaining the estimated gas production, if favorably oriented and dark, but if this is so, then the near-sphericity of the gas outflow at moderate altitudes must be explained.

Finally, the high nucleus-averaged brightness and color temperature of $\approx 350 \text{ K}$ measured from the VEGA spacecraft indicate that icy sublimation cannot cover a dominant fraction of the nucleus. We are left with two possible nucleus models:

Model A: The gas issues from most of the sunlit nucleus surface, at about 350 K, with localized dust production (for obscure reasons) over only 10% of the surface.

Model B: Gas and dust issue from the discrete areas only, which then must be exposed dirty ice at ≈ 200 K, with the rest of the nucleus being inactive at ≈ 350 K [41, 67].

It would seem that a convincing choice between A and B must follow the achievement of both an hydrodynamic modeling of the coma and a consistent modeling of the nucleus. We discuss here only the first part of this objective.

12.2. SPHERICALLY SYMMETRIC MODELS

With the exception of the works discussed in Section 12.3 and 12.4, all existing models assume a spherically symmetric coma (which implies a spherical and isothermal nucleus!). It has become fashionable to express doubts with respect to the significance of any result based on such a simplifying assumption. This is not a correct attitude, for the following reasons:

1. Spherical models can be considered a benchmark for the development of sophisticated methods and the calibration of nonspherical models.
2. The development of comprehensive nonspherical models (i.e., including chemistry and radiative transfer) may prove to be unmanageable.
3. In situ flyby gas density measurements suggest that the gas coma is almost spherically symmetric, at least outside of 1500 km.
4. It has been established that spherically symmetric solutions of the NSEs satisfactorily approximate the exact solution of an axially symmetric outflow in the vicinity of the axis ([3], cited in [16, 20, 48]). Since the vertical from the center of an active region is also the brightest region of the flow, we expect spherical solutions to satisfactorily describe the global properties of a coma produced by a single discrete region. However, proper scaling must be achieved. Let Q_g be the total production, A_{eff} the area of the active region (assumed to be more or less circular), and Ω_{eff} the solid angle subtended by the region from the “nucleus center.” Then, the parametrization of the model must be:

$$R_n^{\text{eff}} = \sqrt{A_{\text{eff}}/\pi} ; Q^{\text{eff}} = Q_g (4\pi/\Omega_{\text{eff}}) \quad (30)$$

with R_n^{eff} being the “effective spherical nucleus radius” and Q^{eff} the “effective spherical production rate.” Notice that R_n^{eff} bears no relation to the nucleus size itself, and that for nucleus model A, $Q^{\text{eff}} \equiv Q_g$, while for nucleus model B, $Q^{\text{eff}} \gg Q_g$! With the exception of [18, 19, 21, 22, 23, 33], all authors adopt R_n^{eff} values unrelated to A_{eff} , and $Q^{\text{eff}} \equiv Q_g$ (even though they may wish to represent a discrete area outflow). The physical justification of (30) is illustrated in, e.g., [3, 85].

5. Possibly, of course, the outcome of a large number of discrete jets can be a nearly spherical gas coma, in which case equation (30) need not necessarily hold. However, in this case, the parameters of an “effective spherical model” that would approximate the multijet coma are yet to be determined.

12.3. TWO-DIMENSIONAL MODELS

Two-dimensional models of a pure gas coma at any altitude [49, 50, 78] and of a dusty coma at low altitudes [45, 46, 52] have been developed. This is the simplest physically possible coma, because even a spherical nucleus gives rise only to an axially symmetric coma. Also, it has been shown that the cylindrically symmetric solution of the NSEs satisfactorily approximates fluid outflow from an elongated slit in the vicinity of the meridian plane [2]. Therefore, these solutions give some information on a coma that would be formed from an elongated crack on the nucleus.

The case of discrete dust emission in an otherwise global gas production (model A) has also been treated in two-dimensional geometry [46].

12.4. THREE-DIMENSIONAL MODELS

A model in which the interaction between the outflows from two distinct active areas is studied has been recently developed [47]. This is, of course, an important step towards a realistic representation of the formation of the coma of Comet Halley (which has, if model B is adopted, three large active areas, plus a number of smaller ones [41]). Figure 12 shows that the interaction between elementary jets results in the formation of standing shock waves enclosing regions of compressed and heated gas. Perhaps the increasing-

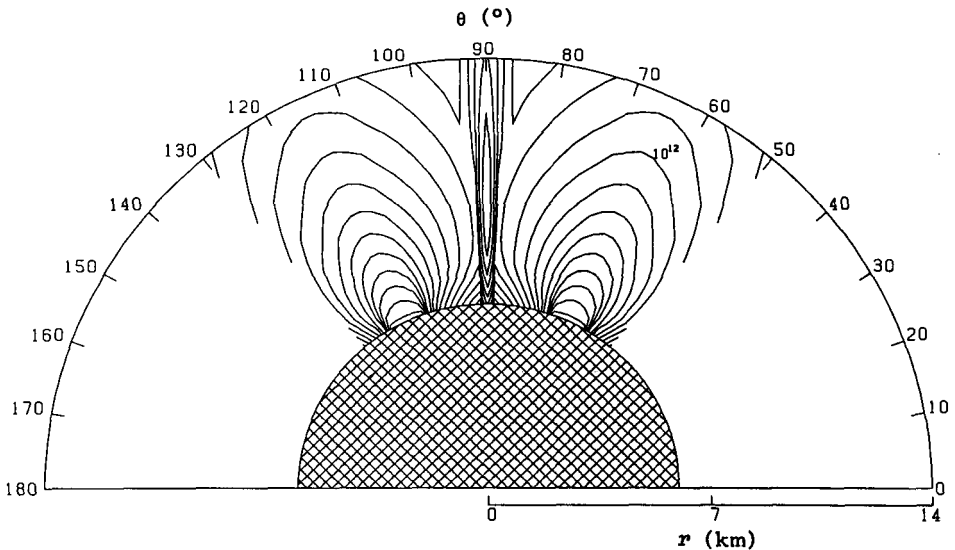


Figure 12. Interaction of two dusty gas jets emanating from a spherical nucleus. The curves are gas isodensity contours equispaced by factors of $10^{0.2}$. Notice the formation of two stationary shocks on the inside boundary of the jets, between which a compressed layer of hot and dense gas is formed. The coma of comet Halley is perhaps formed by more than ten interactions of this kind. From [47].

ly complex structure of the coma induced by many discrete active areas will result in a grossly spherical distribution of gas at high altitudes.

12.5. THE NUCLEUS-COMA INTERFACE

The model A representation (gas outflow across a mantle of dust) has been treated in various ways [31, 52, 67]. The initial gas and dust temperature are strongly dependent upon the solar zenith angle, and the dust temperature exceeds the gas temperature, which is itself far in excess of the ice sublimation temperature [52], so the vapor is undersaturated. In the case of Model B, differing equations must be used for the sublimating areas and for the inactive areas. The ice/vapor interface (active areas) was originally treated by application of free molecular (or “Hertz-Knudsen”) expressions:

$$Z \equiv Z_{HK} = p_S (T_I) / \sqrt{2\pi m_g k_B T_I} \tag{31}$$

with Z being the sublimation rate (molecules/cm² s) and T_I the ice surface (not the vapor) temperature. By definition, however, this expression excludes any hydrodynamic treatment of the coma, since collisionless conditions are assumed! For typical sublimation rates, Z_{HK} is, indeed, the rate of emission of the ice surface, but since the m.f.p. does exceed the active area size, a fraction α of the emitted molecules is evidently backscattered toward the ice, where it is recondensed. One must write [17, 67, 72, 85]:

$$Z \equiv Z_{HK} (1 - \alpha) \tag{32}$$

It is essential to observe that:

1. α cannot be a function of T_I alone, since one can indeed “pump” various amounts of vapor from a surface at T_I : with an extremely powerful pump, one can reach $\alpha = 0$, while in a closed tank (equilibrium condition), $\alpha = 1$. Therefore, α depends upon the subsequent history of the vapor.
2. When $\alpha \neq 1$, the gas d.f. near the surface is non-Maxwellian; in effect, the surface always emits molecules with a half-space Maxwellian d.f., while back-scattered molecules have differing d.f. dependent upon α , which insure differing return fluxes. Therefore, hydrodynamic equations cannot be used close to the surface, but only sufficiently far from it. The initial gas parameters ρ_0, T_0, V_0 apply at that distance where the d.f. starts to assume a Maxwellian shape. By solving an approximate CBE, one can show that this distance is about 10 m.f.p., i.e., less than 1 m for Halley flyby conditions [17, 85].

At any value of α , it is required that the mass, momentum, and energy carried away by the fluid be equal to the net mass, momentum, and energy leaving the ice surface, i.e., those corresponding to Z_{HK} minus those recondensed. The former are computable from a half-space Maxwell-Boltzman function normalized by p_S and T_I . As a first-order approximation, the latter are computable from a half-space drifting Maxwellian d.f. with parameters ρ_0, T_0, V_0 . We end up with functions $\rho_0(\alpha), T_0(\alpha), V_0(\alpha)$. Since the solution of the

coma hydrodynamic equations gives the flow initial Mach number M_0 , it is more sensible to use M_0 as the free parameter. If the presence of dust is neglected, we get the following relations [17]:

$$T_0/T_I = \left[\sqrt{1 + \frac{1}{4} \left(S_M \frac{\gamma_0 - 1}{\gamma_0 + 1} \right)^2} - \frac{\sqrt{\pi}}{2} \left(S_M \frac{\gamma_0 - 1}{\gamma_0 + 1} \right) \right]^2 \quad (33)$$

$$p_0/p_s(T_I) = \frac{1}{2} - S_M \sqrt{\frac{T_0}{\pi T_I}} + \left[\left(S_M^2 + \frac{1}{2} \right) \sqrt{\frac{T_0}{T_I}} - \frac{S_M}{2} \sqrt{\pi} \right] \operatorname{erfc}(S_M) \exp(S_M^2) \quad (34)$$

with:

$$S_M = M_0 \sqrt{\gamma_0/2} \quad (35)$$

and α given by:

$$\alpha = 1 - M_0 [p_0/p_s(T_I)] \sqrt{2\pi\gamma_0(T_I/T_0)} \quad (36)$$

Typically (near $M_0 = 1$), one has $p_0/p_s(T_I) \approx 0.2$, $T_0/T_I \approx 0.8$, and $\alpha \approx 0.2$. An accurate experimental verification of this simple theory has been provided recently by direct laser fluorescence measurements of the d.f. of sublimating iodine molecules [54]. The use of expressions (33) to (36) commends itself for precise assessment of the nongravitational forces [67] and for a realistic assessment of the water recondensation [17, 21]. These expressions have been recently generalized to the case of dusty sublimation [85]. In this case, one finds that, in comparison with equations (33) to (36), the ratios T_0/T_I is slightly increased, and the ratio $p_0/p_s(T_I)$ slightly decreased.

As any other nonequilibrium region of a fluid, the solid/gas sublimation interface region can be modelled by DMC simulation [63]. The first simulation of this kind has appeared recently [5]. It confirms the existence of a disequilibrium region with thickness ≈ 10 m.f.p., where the gas velocity distribution is highly nonspherical. However, the values found for α (≈ 0.13) and for T_0/T_I (0.56) are not in very good agreement with those obtained from equations (34) to (37), and the d.f. is found to correspond to $T_{\parallel} \ll T_{\perp}$, in contradiction with analytic predictions and with experiments [54].

Since the non-icy hot parts of the nucleus are assumed in model B to be inactive, the coma/surface interaction there is the classical problem of flow over a wall with the temperature differing from the gas temperature: there is heat input into the gas and viscous deceleration. A comprehensive treatment is not available at this time because over the inactive areas, the gas density gradients are necessarily strong and the viscosity effects become dominant [46]. A rarefied gas dynamic treatment (based on the solution of a CBE) is required. Therefore, at the present time, too strong conclusions from any treatment of the model B case, concerning lateral transport of the gas, appear premature.

13. On the Reliability of the Conclusion of Present Models

Table 2 summarizes the key features of the hydrodynamic models reviewed in this study.

To the extent that identification and illustration of the key processes at work in the coma are concerned, one can perhaps conclude that existing models make it possible to understand the formation of a coma. However, the authors, probably under the pressure of cometary observers, typically include in their publications conclusions of a much stronger character; for instance, qualitative fits to high-resolution data are presented as validations of all the assumptions and approximations incorporated in the work. If, however, critical intercomparison of the works is made [20], we discover that the assumptions, approximations, and even parameter values are sometimes mutually contradictory. We are thus tempted to conclude “not only do we understand the formation of a coma, but we can model it in so many ways that no strong conclusions can be drawn from even refined fits to existing data” [20].

The inner coma parameters that are best suitable for checking the mutual consistency of models are the gas, ion, and electron temperatures [20]. Unfortunately, they cannot be used to discriminate amongst conflicting models, because their accurate measurement requires in situ experiments that are presently lacking. We therefore choose to discuss the relevance of present models with a few other selected examples.

13.1. TERMINAL DUST VELOCITIES

Figure 13 presents the size dependence of the terminal velocity of spherical dust grains computed by two multicomponent dust models, one using a “model A” nucleus surface [29], and the other a “model B” surface [15]. The other parameters are selected to approximate Halley flyby conditions. The agreement is evident, but somewhat misleading. The cutoff size itself is very uncertain (Figure 5). Many effects contribute to make the dust velocity increasingly uncertain with size:

1. Grain density uncertainty.
2. Grain asphericity.
3. Local variations in the local gas outflow rate over the nucleus.
4. Short-term variations in the gas production.

These variations may be negligible in shaping the gas coma, but not in setting the dust velocity, which is a rapid phenomenon. Finally, it should be noted that the concept of “a” dust terminal velocity has its origin in the development of spherically symmetric models of the coma; in the case of gas production from discrete areas, some divergence of the dust flow is expected (see Section 13.2 and the review in this book by T.I. Gombosi) and has indeed been observed on the Giotto images [77]. This effect also implies a spread in grain velocity. Perhaps the only safe conclusion concerning large grains is that their velocity is bound by the minimum escape velocity and the maximum adiabatic gas velocities, i.e.:

$$\sqrt{2GM_n/(R_n)_{\min}} < V_d < \sqrt{\frac{\gamma_0 + 1}{\gamma_0 - 1} \gamma_0 k_B \frac{T_{\max}}{m_g}} \tag{37}$$

Table 2. Critical Physical Assumptions of Recent Multifluid Models

Initial Boundary Conditions

Icy sublimation:

Ad hoc parameters values	6, 7, 11, 12, 14, 15, 24, 35, 36, 40, 44, 45, 46, 50, 58, 60, 69
Correct interface equations	17, 18, 21, 23
Mantle outgassing	29, 30, 52

Dust Properties

No dust	6, 7, 11, 13, 14, 24, 35, 36, 40, 44, 50, 69, 78
Crude optical properties	12, 29, 30, 45, 46, 52
Realistic optical properties	15, 17, 18, 21, 23, 58, 60
One mineralic type	12, 29, 30, 45, 52, 58, 60
Several mineralic types	15, 17, 18, 21, 23
Volatile grains	15
Single size grains	12, 15, 17, 21, 30, 45, 52, 58, 60
Small number of grain sizes	46, 47
Realistic size spectrum	18, 23, 29

Water Photodissociative Heating

Omitted	44
Constant through coma	24, 29, 30, 50, 52, 60, 78
Altitude dependent:	
Analytic	7, 15, 17, 18, 21, 23, 35, 36, 45, 46, 58, 69
Monte Carlo	6, 7, 11, 12, 13, 40

Water Radiative Loss

Omitted	15, 17, 18, 21, 40, 44, 52
Single molecule loss [57]	30, 40, 45, 46, 50, 58, 60, 78
Single molecule loss + coma attenuation [30]	11, 12, 13, 29, 35, 36, 69
Realistic treatment	6, 7, 23, 24

Strong Water Radiative Heating From Dust

29, 57, 60

Water Recondensation

17, 21, 23, 44

Viscosity and Thermal Conductivity Terms

45, 46, 47

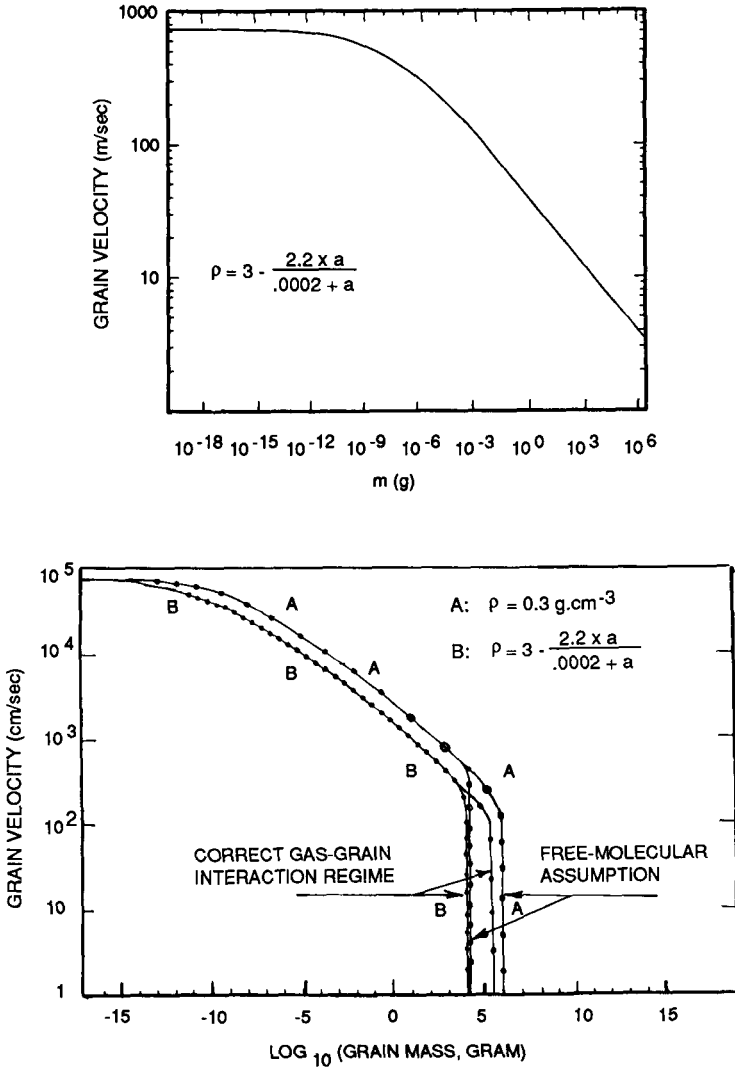


Figure 13. Terminal dust velocities computed by two independent multicomponent dusty hydrodynamic models for Halley flyby conditions ([29], top, and [18], bottom). The two models differ by almost all their detailed assumptions (see Table 2 and quoted references), but nonetheless indicate remarkable agreement. Notice that the use of the free-molecular theory overestimates the maximum ejectable mass by two orders of magnitude! Notice also that the uncertainty resulting from variations in grain density by far exceeds the difference between the two results shown here.

For Halley flyby conditions ($(R_n)_{\min} \approx 3.5$ km, $M_n \approx 3 \times 10^{17}$ g, and $T_{\max} \approx 350$ K), these limits are ≈ 3.4 m/s and ≈ 0.9 km/s. In any case, each large grain probably can assume a large interval of ejection velocities. Strong conclusions ignoring this fact should be avoided.

Recently, the analysis of dust tail brightness has been used to infer “average” dust velocities over the size range of 10 μm to 2 mm [27, 28], with little agreement with the size dependence shown on Figure 13: the derived size dependence is much flatter. This could be due in part to the expected large velocity spread in individual grain velocities. However, it is suggested in [28] that grain fragmentation is responsible for this discrepancy: if intermediate-size grains come from initially large aggregates, they will receive from the gas only a small velocity increase above that of their slow parent, and the size dependence of the velocity will be small.

13.2. GAS VELOCITIES

In contrast with the case of the dust velocity, there exist one in situ determination of the water outflow velocity [53] and several indirect coma-average velocity determinations based on the Doppler effect, both for water [82] and for some other molecules. Also, observation of the radial motion of shells of CN yields radial velocities for that molecule [40, 48, 70]. We will return to the case of CN in the next section, and restrict ourselves here to H_2O velocities.

Figure 14 presents in situ measured velocities [53], post-perihelion coma integrated values [82], and a number of hydrodynamic model determinations [12, 23, 40], plus the result from the already discussed DMC simulation [33]. Analysis of this figure suggests the following:

1. Although the remote sensing and in situ data correspond to about the same water production rate, they are not in mutual agreement. This annoying discrepancy does not seem to have attracted much attention, with the consequence that it is presently unexplained.
2. All model computations, as well as the in situ data, indicate an uninterrupted increase of the outflow velocity throughout the water coma. Nowhere do we see anything indicative of a “collision sphere.” Therefore, the ubiquitous expression “the” gas outflow velocity has no meaning (unless we want to speak only of order of magnitudes). We can speak only of “the” gas velocity “at” a position in the coma. For instance, the remote coma-integrated determination really concerns a shell in the water coma wherefrom, say, 90% of the emission originates; our error box on Figure 14 is based on the approximate r^{-1} dependence of the coma brightness and on the instrument field of view.
3. Two of the recondensation-free results indicate a nearly constant velocity out to 10^4 km [33, 40] (at about 0.75 km/s), while the two other ones [12, 23] indicate a steep rise with the distance starting already at 10^3 km (with values 1.2 and 1.0 km/s at 10^4 km). The model assumptions are very different of course (see Table 2), but the precise reasons for such discrepancies remain to be found out.
4. Assuming “model A” water production ($Q_{\text{eff}} = Q$), none of the models can fit the remote sensing data. As regards the in situ results, they are in rough agree-

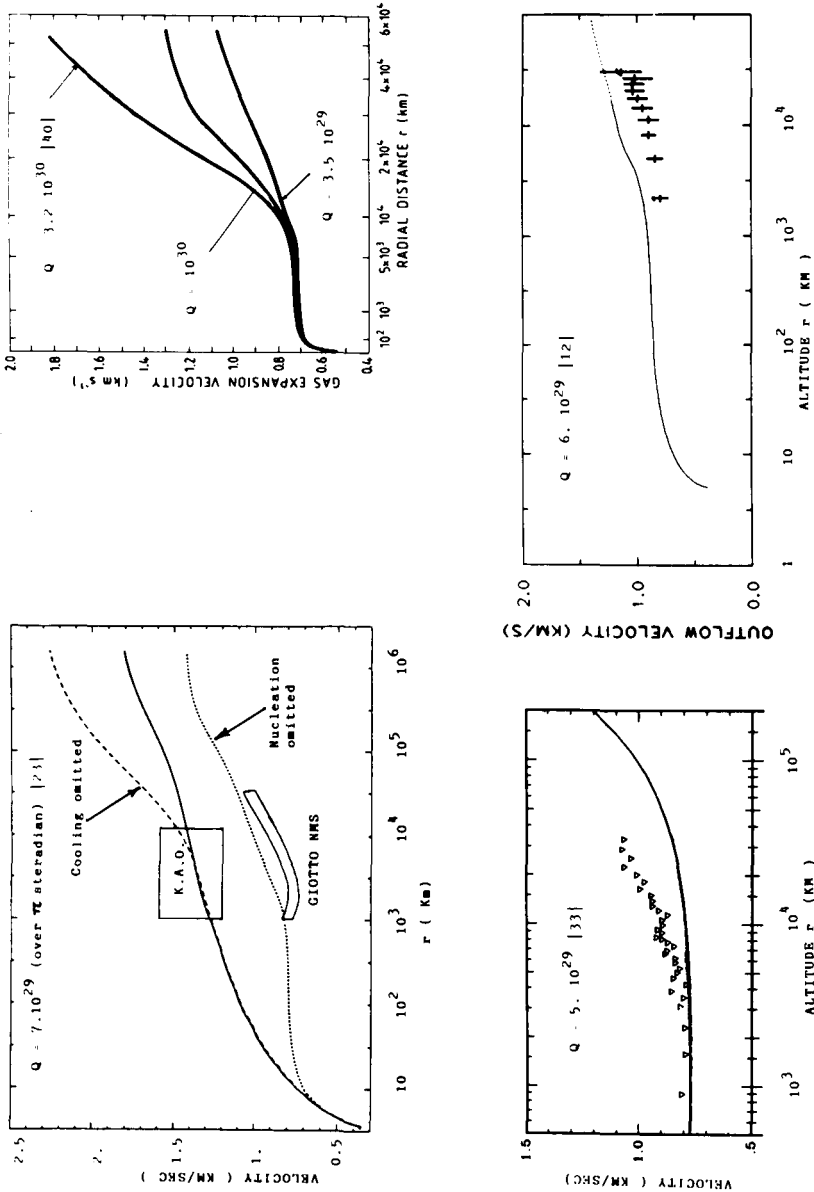


Figure 14. Comet P/Halley water outflow velocities at the time of the flyby observations. Crosses (lower panel, right), triangles (lower panel, left) and the band labeled "Giotto NMS" refer to the same in situ measurements [53]. The rectangle labeled "KAO" shows the remote sensing measurement [82]. All curves are model computations. The assumed water production rate Q is indicated. Spherical outflow (over 4π steradian) is assumed, except for the results of the upper left panel.

ment with all the nucleation-free computations (but exact fits are out of reach in view of the model uncertainties discussed in Sections 8 and 9).

5. Assuming “model B” water production ($Q_{\text{eff}} = 4 Q$), comparison is possible only with the computations of [23] and [40]. The in situ results agree roughly with the nucleation-free computations [23, 40], and the remote sensing results with the computation that takes nucleation into account!

At least one conclusion is evident: authors must show results at several values of Q if any valuable comparison with data is to be made. For the present time, only qualitative information can be extracted from the available publications, and, above all, it is impossible to discriminate between the conflicting model assumptions.

13.3. SPHERICITY OR ASPHERICITY OF THE GAS OUTFLOW?

As indicated earlier, in situ and remote sensing observations of H_2O favor moderate asphericity, if any, of the gas outflow (outside 10^3 km). The observation of apparently spherical CN and C_2 shells reinforces that impression. But it is not easy to reconcile isotropic flow with the near-nucleus dust environment. Unless we make the ad hoc assumption of inhomogeneous dust distribution inside otherwise homogeneous active areas, the observations of a number of tiny dust “jets” suggests that the gas production is also highly aspherical.

The observation of both long-lasting CN jets and expanding spherical CN halos is even more puzzling. A detailed discussion is included in [48]. Regardless of whether one is observing a tracer of active grains or of dissociating molecules, it is hard to avoid the conclusion that their production is sometimes isotropic, that it is sometimes localized, or, alternatively, that an unknown isotropization process is sometimes effective and sometimes ineffective. (In passing, let us remark that the unrelated attempts to use the collision sphere concept to evaluate the CN jet divergence [11] or the CN shell velocities [40, 70] should be regarded with skepticism: we do not see how water could assume a transition regime outflow without remaining coupled to all other minor molecules in the coma.)

It is a fundamental property of supersonic gas jets that the geometrical properties of the source are preserved far out. Figure 15 presents results from the two nonspherical models of the water coma that extend to high altitudes [49, 50, 78]. They agree spectacularly in predicting the preservation, at all altitudes, of smooth surface gas production asymmetries. To be sure, these models use inviscid equations, which are less suitable for dealing with transition regime flow, and we do not know to what extent viscous effects would reduce the asymmetries. But, recently, a direct Monte Carlo simulation of water outflow under similar assumptions has appeared, and it is in excellent agreement with the hydrodynamic results (see Figure 15) [34].

On the other hand, a number of physical processes that probably take place at very low altitudes in a coma violate the preservation of flow geometry:

1. If (as suggested by some authors [81]) a large fraction of the coma water issues from volatile grains originating from a localized area of the nucleus, the asymptotic gas flow pattern should resemble a spherical flow from the peak source region (i.e., from grains within 1000 km from the surface).

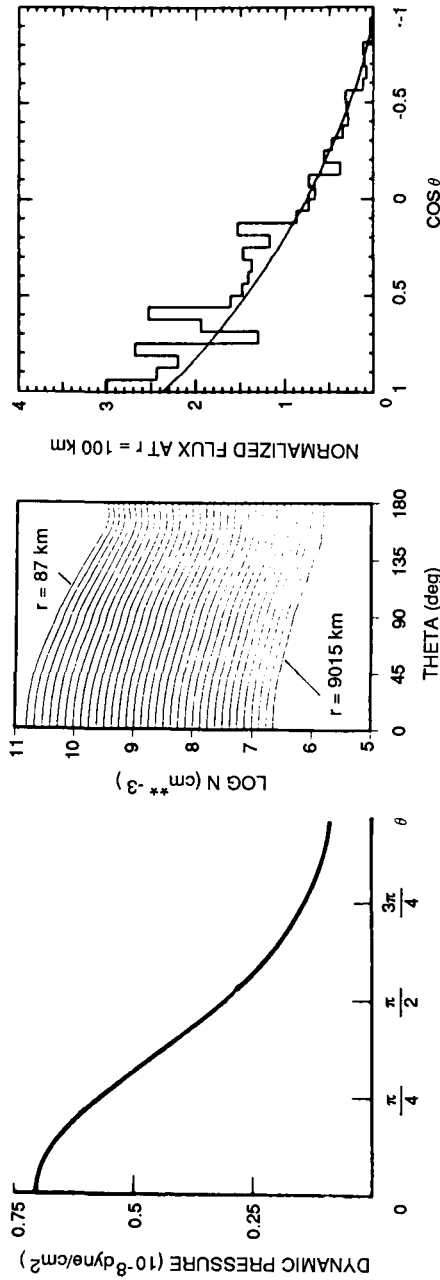


Figure 15. Preservation of gas production asymmetries in the coma, in the case of a single jet outflow. For the three results shown, a $\cos(\theta)$ production law is assumed, with θ being the solar zenith angle. The total production rate is chosen to approximate Comet Halley flyby conditions. Left: Dynamic pressure at an altitude of 10^4 km [78]. Middle: Density curves at various altitudes [49]. These two independent results use inviscid equations. Right: Relative flux at an altitude of 100 km. Here, the result was obtained by a direct Monte Carlo simulation, and the solid curve shows the collisionless limit [34].

2. Addition of mass, momentum, or energy into a supersonic flow may produce a shock deceleration of the flow with associated flow divergence. One of the possible processes of this kind is supercritical recondensation (Section 10.1).
3. It has been suggested recently [42] that heavy mass loading of the subsonic gas (just above the nucleus surface) by fragmenting fine dust could delay the sonic transition of the flow up to altitudes as high as 2 to 4 km (as opposed to ≈ 1 m as found in Section 7.3 for P/Halley, and to ≈ 100 m as found by authors who attribute all the dust loss to single-size small grains). In this case, lateral (subsonic) flow of the gas is to be expected. The numerical results [42] certainly depend critically upon the strong assumption of an initial dust-to-gas ratio of 3 being entirely blocked into micrometer-size grains. Therefore, in order to be really convincing, an hydrodynamic model of P/Halley with fragmenting dust should also be capable of predicting the in situ measured very broad "asymptotic" size distribution.
4. The interaction between a number of initially individual supersonic jets may perhaps lead, within less than $\approx 10^2$ km, to a coma with a roughly spherically symmetric appearance (and a number of fine structures averaged out by remote sensing). This is suggested by the recent hydrodynamic simulation of the interaction between two dusty jets 50° apart on a spherical nucleus ([47] and Figure 12). The jets are separated by two standing shock fronts, between which a layer of subsonic gas is formed. At high enough altitudes, the density isocontours tend to resemble those of a single broad jet with superimposed density and temperature fluctuations.

Acknowledgments

Drs. Combi, Fulle, Gombosi, Hodges, Ip, Kitamura, Kömle, Marconi, Rickman, Szegö, and Ytrehus are thanked for communication of some of their works prior to publication. Ms. G. Bargot-Despontin is thanked for efficient editing of the manuscript.

References

1. Allen, M., Delitsky, M., Huntress, W., Yung, Y., Ip, W.-H., Schwenn, R., Rosenbauer, H., Shelley, E., Balsiger, H., and Geiss, J. (1987). 'Evidence for methane and ammonia in the coma of comet Halley,' *Astron. Astrophys.* 187, 502–512.
2. Anderson, J.B., Foch, J.D., Shaw, M.J., Stern, R.C., and Wu, B.J. (1986). 'Monte Carlo simulation of free-jet flow from a slit,' in C. Cercignani and V. Boffi (eds.), *Rarefied Gas Dynamics XV*, Teubner Press, Stuttgart, Vol. 1, pp. 442–451.
3. Ashkenas, H., and Sherman, T.S. (1966). 'The structure and utilization of supersonic free-jets in low-density wind tunnels,' in J.H. de Leeuw (ed.), *Rarefied Gas Dynamics IV*, Academic Press, New York, Vol. 2, pp. 84–105.
4. Banaskiewicz, M., Marconi, M., Kömle, N.I., and Ip, W.H. (1989). 'Dynamics of large grains around Halley's comet,' poster presented at "Comets in the Post-Halley Era," Bamberg, F.R.G.

5. Bisikalo, D.V., Marov, M.Ya., Shematovich, V.I., and Strel'nitsky, V.S. (1989). 'The flow of the subliming gas in the near-nuclear (Knudsen) layer of the cometary coma,' *Adv. Space Res.* 9 (3), 53–58.
6. Bockelee-Morvan, D. (1987). 'A model for the excitation of water in comets,' *Astron. Astrophys.* 181, 169–181.
7. Bockelee-Morvan, D., and Crovisier, J. (1987). 'The role of water in the thermal balance of the coma,' *ESA SP-278*, pp. 235–240.
8. Burgers, J.M. (1969). *Flow Equations for Composite Gases*, Academic Press, New York.
9. Campbell, D.B., Harmon, J.K., and Shapiro, I.I. (1989). 'Radar observations of comet Halley,' *Astrophys. J.* 338, 1094–1105.
10. Cattolica, R., Robben, F., Talbot, L., and Willis, D.R. (1974). 'Translational non-equilibrium in free-jet expansion,' *Phys. Fluids*, 17 (10), 1793–1807.
11. Combi, M.R. (1987). 'Sources of cometary radicals and their jets: Gases or grains,' *Icarus* 71, 178–191.
12. Combi, M.R. (1989). 'The outflow speed of the coma of Halley's comet,' *Icarus* 81, 41–50.
13. Combi, M.R., and Smyth, W.H. (1988). 'Monte Carlo particle trajectory models for neutral coma gases. I. Models and equations,' *Astrophys. J.* 327, 1026–1043; and Combi, M.R., and Smyth, W.H. (1988). 'Monte Carlo particle trajectory models for neutral coma gases. II. The spatial morphology of the Lyman alpha coma,' *Astrophys. J.* 327, 1044–1059.
14. Cravens, T.E. (1989). 'A magnetohydrodynamic model of the inner coma of Comet Halley,' *J. Geophys. Res.* 94 (A11), 15,025–15,040.
15. Crifo, J.F. (1986a). 'Hydrodynamic expansion of cometary gas loaded with refractory and volatile grains,' in C.I. Lagerkvist et al. (eds.), *Asteroids, Comets, Meteors II*, Reprocentralen HSC, Uppsala, pp. 389–392.
16. Crifo, J.F. (1986b). 'Comets as dirty snowballs sublimating in empty space,' in C. Cercignani and V. Boffi (eds.), *Rarefied Gas Dynamics XV*, Teubner Press, Stuttgart, pp. 229–250.
17. Crifo, J.F. (1987a). 'Improved gas kinetic treatment of cometary water sublimation and recondensation, application to comet P/Halley,' *Astron. Astrophys.* 187, 438–450.
18. Crifo, J.F. (1987b). 'Optical and hydrodynamic implications of Comet Halley dust size distribution,' *ESA SP-278*, pp. 399–408.
19. Crifo, J.F. (1987c). 'Are cometary dust mass loss rates deduced from optical emissions reliable?', in Z. Ceplecha and P. Pecina (eds.), *Interplanetary Matter*, Proceedings of the Xth ERAM IAU Meeting, Prague, Czechoslovakia, Czechoslovak Academy of Sciences report G7, pp. 59–66.
20. Crifo, J.F. (1989). 'Collisional coma models: An unorthodox overview,' *Adv. Space Res.* 9 (3), 197–211.
21. Crifo, J.F. (1990a). 'Water clusters in the coma of Comet Halley and their effect on the gas density, temperature and velocity,' *Icarus*, in press.
22. Crifo, J.F. (1990b). 'A realistic simple size approximation to Comet Halley dust size distribution, suitable for hydrodynamic applications,' preprint.

23. Crifo, J.F., Crovisier, J., and Bockelee-Morvan, D. (1989). 'Proposed water velocity and temperature radial profiles appropriate to Comet Halley flyby conditions,' poster presented at "Comets in the Post-Halley Era," Bamberg, F.R.G.
24. Crovisier, J. (1984). 'The water molecule in comets: Fluorescence mechanisms and thermodynamics of the inner coma,' *Astron. Astrophys.* 130, 361–372.
25. Crovisier, J. (1989). 'The photodissociation of water in cometary atmospheres,' *Astron. Astrophys.* 213, 459–464.
26. Festou, M. (1981). 'The density distribution of neutral compounds in cometary atmospheres,' *Astron. Astrophys.* 95, 69–79.
27. Fulle, M. (1989). 'Evaluation of cometary dust parameters from numerical simulations: Comparison with analytical approach and role of anisotropic emissions,' *Astron. Astrophys.* 217, 283–297.
28. Fulle, M. (1990). 'A neck-line structure in the dust tail of comet 1910 I,' preprint.
29. Gombosi, T.I. (1986). 'A heuristic model of the Comet Halley dust size distributions,' *ESA SP-250*, pp. 167–171.
30. Gombosi, T.I., Cravens, T.E., and Nagy, A.F. (1985). 'Time-dependent dusty gas dynamical flow near cometary nuclei,' *Astrophys. J.* 293, 328–341.
31. Gombosi, T.I., Nagy, A.F., and Cravens, J.E. (1985). 'Dust and neutral gas modeling of the inner upper atmosphere of comets,' *Rev. Geophys.* 24, 667–700.
32. Gustafson, B.A. (1989). 'Comet ejections and dynamics of nonspherical dust particles and meteoroids,' *Astrophys. J.* 337, 945–949.
33. Hodges, R.R. (1990a). 'Monte Carlo simulation of nonadiabatic expansion in cometary atmospheres: Halley,' *Icarus* 83, 410–433.
34. Hodges, R.R. (1990b). 'Aspheric flow of water vapor in cometary atmospheres,' preprint.
35. Huebner, W.F. (1985). 'The photochemistry of comets,' in J.J. Levine (ed.), *The Photochemistry of Atmospheres*, Academic Press, Orlando, pp. 438–508.
36. Huebner, W.F., and Keady, J.J. (1983). 'Energy balance and photochemical processes in the inner coma,' in T.I. Gombosi (ed.), *Cometary Exploration*, Academy of Hungary Press, Budapest, pp. 165–183.
37. Huebner, W.F., and Keady, J.J. (1984). 'First-flight escape from spheres with r^{-2} density distribution,' *Astron. Astrophys.* 135, 177–180.
38. Ip, W.H. (1983). 'Photochemical heating of the cometary plasma,' *Astrophys. J.* 264, 726–732.
39. Ip, W.H. (1986). 'Photochemical heating of comets: The effect of icy water droplet recondensation,' *Astrophys. J.* 300, 456–460.
40. Ip, W.H. (1989). 'Photochemical heating of cometary gases: III. The radial variation of the expansion velocity of CN shells in Comet Halley,' *Astrophys. J.* 346, 475–480.
41. Keller, H.U., Delamere, W.A., Huebner, W.F., Reitsema, H.J., Schmidt, H.U., Whipple, F.L., Wilhelm, K., Curdt, W., Kramm, R., Thomas, N., Arpigny, C., Barbieri, C., Bonnet, R.M., Cazes, S., Coradini, M., Cosmovici, C.B., Hughes, D.W., Jamar, C., Malaise, D., Schmidt, K., Schmidt, W.K.H., and Seige, P. (1987). 'Comet P/Halley's nucleus and its activity,' *Astron. Astrophys.* 187, 807–823.

42. Keller, U.H., Marconi, M.L., and Thomas, N. (1990). 'Hydrodynamic implications of particle fragmentation near cometary nuclei,' *Astron. Astrophys.* 227, L1–L4.
43. Kitamura, Y., Ashihara, U., and Yamamoto, T. (1985). 'A model for the hydrogen coma of a comet,' *Icarus* 61, 278–295.
44. Kitamura, Y., and Yamamoto, T. (1986). 'Hydrodynamic study of condensation and sublimation of ice particles in cometary atmospheres,' *Icarus* 68 (2), 266–275.
45. Kitamura, Y. (1986). 'Axisymmetric dusty gas jet in the inner coma of a comet,' *Icarus* 66, 241–257.
46. Kitamura, Y. (1987). 'Axisymmetric dusty gas jet in the inner coma of a comet. II. The case of isolated jets,' *Icarus* 72, 555–567.
47. Kitamura, Y. (1988). 'Numerical study of 3-dimensional cometary jets: Formation of shock waves in cometary atmospheres,' in *Proceedings of the XXth ISAS Lunar and Planetary Symposium, Tokyo*, pp. 33–34. Also, preprint (1989).
48. Kömle, N.I. (1990). 'Jet and shell structures in the cometary coma,' in J. Mason (ed.), *Comet Halley 1986: Worldwide Investigations, Results and Interpretations*, J. Wiley, New York, in press.
49. Kömle, N.I., and Ip, W.H. (1987a). 'A model for the anisotropic structure of the neutral gas coma of a comet,' *ESA SP-278*, 247–254.
50. Kömle, N.I., and Ip, W.H. (1987). 'Anisotropic non-stationary gas flow dynamics in the coma of Comet P/Halley,' *Astron. Astrophys.* 187, 405–410.
51. Körösmezey, A., Cravens, T.E., Gombosi, T.I., Nagy, A.F., Mendis, D.A., Szegő, K., Gribov, B.E., Sagdeev, R.Z., Shapiro, V.D., and Shevchenko, V.I. (1987). 'A new model of cometary ionospheres,' *J. Geophys. Res.* 92 (A7), 7331–7340.
52. Körösmezey, A., and Gombosi, T.I. (1990). 'A time-dependent dusty-gas dynamic model of axisymmetric cometary jets,' *Icarus*, 84, 118–153.
53. Lämmerzahl, P., Krankowsky, D., Hodges, R.R., Stubbemann, U., Woweries, J., Herrwerth, I., Berthelier, J.J., Illiano, J.M., Eberhardt, P., Dolder, U., Schulte, W., and Hoffman, J.H. (1987). 'Expansion velocity and temperature of gas and ions measured in the coma of Comet P/Halley,' *Astron. Astrophys.* 187, 169–173.
54. Mager, R., Adomeit, G., and Wortberg, G. (1989). 'Theoretical and experimental investigation of the strong evaporation of solids,' in E.P. Muntz et al. (eds.), *Rarefied Gas Dynamics: Space Related Studies, Progress in Astronautics and Aeronautics*, Vol. 118, AIAA Press, Washington, D.C., pp. 460–469.
55. Mc Donnell, J.A.M., Alexander, W.M., Burton, W.M., Bussoletti, E., Evans, G.C., Evans, S.T., Firth, J.G., Gard, R.J.L., Green, S.F., Grun, E., Hanner, M.S., Hughes, D.W., Igenbergs, E., Kissel, J., Kuczera, H., Lindblad, B.A., Langevin, Y., Mandeville, J.-C., Nappo, S., Pankiewicz, G.S.A., Perry, C.H., Schwehm, G.H., Sekanina, Z., Stevenson, T.J., Turner, R.F., Weishaupt, U., Wallis, M.K., and Zarnecki, J.C. (1987). 'The dust distribution within the inner coma of comet P/Halley 1982i: Encounter by Giotto's impact detectors,' *Astron. Astrophys.* 187, 719–741.
56. McIntosh, B.A., and Jones, J. (1988). 'The Halley comet meteor stream: Numerical modelling of its dynamical evolution,' *Mon. Not. R. Astr. Soc.* 235, 673–693.
57. Marconi, M.L. (1986). 'The effect of dust IR and H₂O IR on the thermodynamics of Comet Halley's atmosphere,' unpublished UCSD report.

58. Marconi, M.L., and Mendis, D.A. (1983). 'The atmosphere of a dirty clathrate cometary nucleus: A two phase multifluid model,' *Astrophys. J.* 273, 381–396.
59. Marconi, M.L., and Mendis, D.A. (1984). 'The effects of the diffuse radiation fields due to multiple scattering and thermal reradiation by dust on the dynamics and thermodynamics of a dusty cometary atmosphere,' *Astrophys. J.* 287, 445–454.
60. Marconi, M.L., and Mendis, D.A. (1986). 'Infrared heating of Comet Halley's atmosphere,' *The Moon and Planets*, 36, 249–256.
61. Mazets, E.P., Sagdeev, R.Z., Aptekar, R.L., Golenetskii, S.V., Guryan, Yu.A., Dyachkov, A.V., Ilyinskii, V.N., Panov, V.N., Petrov, G.G., Savvin, A.V., Sokolov, I.A., Frederiks, D.D., Khavenson, N.G., Shapiro, V.D., and Shevchenko, V.I. (1987). 'Dust in comet P/Halley from Vega observations,' *Astron. Astrophys.* 187, 699–706.
62. Mendis, D.A., Houppis, L.F., and Marconi, M.L. (1985). 'The physics of comets,' *Fundam. Cosm. Phys.* 10, 1–379.
63. Muntz, E.P. (1989). 'Rarefied gas dynamics,' *Ann. Rev. Fluid Mech.* 21, 387–417.
64. Olsson-Steel, D. (1987). 'The dispersal of meteoroid streams by radiative effects,' in Z. Ceplecha and P. Pecina (eds.), *Interplanetary Matter, Proceedings of the Xth ERAM IAU Meeting, Prague, Czechoslovakia, Czechoslovak Academy of Sciences report G7*, pp. 157–161.
65. Peyret, R., and Viviand, H. (1976). 'Computations of viscous compressible flows based on the Navier Stokes Equation,' *Nato AGARD publication AG 212*.
66. Probst, R.F. (1969). 'The dusty gas dynamics of comet heads,' in M.A. Lavrentiev (ed.), *Problems of Hydrodynamics and Continuum Mechanics*, SIAM, Philadelphia, pp. 568–583.
67. Rickman, H. (1989). 'The nucleus of Comet Halley: Surface, structure, mean density, gas and dust production,' *Adv. Space Res.* 9 (3), 59–72.
68. Salo, H. (1988). 'Monte Carlo modelling of the net effects of coma scattering and thermal reradiation on the energy input to cometary nucleus,' *Icarus* 76 (2), 253–269.
69. Schmidt, H.U., Wegmann, R., Huebner, W.F., and Boice, D.C. (1988). 'Cometary gas and plasma flow with detailed chemistry,' *Comput. Phys. Comm.* 49 (1), 17–59.
70. Schulz, R., and Schlosser, W. (1989). 'CN-shell structures and dynamics of the nucleus of Comet P/Halley,' *Astron. Astrophys.* 214, 375–385.
71. Shimizu, M. (1976). 'The structure of cometary atmospheres, I. Temperature distribution,' *Astrophys. Space Sci.* 40, 149–155.
72. Shul'man, L.M. (1970). 'The physical conditions in the boundary layer of a cometary nucleus,' *Astron. Astrophys.* 4, translated as NASA-N70-30776, pp. 100–109.
73. Shul'man, L.M. (1972). 'Dinamika Kometnikh Atmosfer Neitralnii Gas,' *Naukova Dumka, Kiev*, pp. 170–173 (in Russian).
74. Sykes, M.V. (1988). 'Observations of extended zodiacal structures,' *Astrophys. J.* 334, L55–L58.
75. Szegő, K., Toth, I., Szatmary, Z., Smith, B.A., Kondor, A., and Merenyi, E. (1989). 'Dust photometry in the near nucleus region of Comet Halley,' submitted to *Icarus*.

76. Thomas, N., and Keller, U.H. (1987). 'Fine dust structures in the emission of comet P/Halley observed by the Halley Multicolour Camera on board Giotto,' *Astron. Astrophys.* 187, 843–846.
77. Thomas, N., and Keller, U.H. (1990). 'Interpretation of the inner coma observations of Comet P/Halley by the Halley Multicolor Camera,' *Ann. Geophys.* 8, 147–166.
78. Vergazov, M.A., and Krasnobaev, K.V. (1985). 'Axisymmetric flow of reacting gas from a comet nucleus,' *Sov. Astron. Lett.* 11 (4), 232–235.
79. Vincenti, W.G., and Kruger, C.H. (1975). *Introduction to Physical Gas Dynamics*, J. Wiley, New York.
80. Wallis, M.K. (1982). 'Dusty gas dynamics in real comets,' in L.L. Wilkening (ed.), *Comets*, University of Arizona Press, Tucson, pp. 357–369.
81. Wallis, M.K., Rabilizirov, R., and Wickramasinghe, N.C. (1987). 'Evaporating grains in P/Halley's coma,' *Astron. Astrophys.* 187, 801–806.
82. Weaver, H.A., and Mumma, M.J. (1987). 'Infrared investigations of water in Comet P/Halley,' *Astron. Astrophys.* 187, 411–418.
83. Wegman, R., Schmidt, H.U., Huebner, W.F., and Boice, D.C. (1987). 'Cometary MHD and chemistry,' *Astron. Astrophys.* 187, 339–350.
84. Wu, Z.J. (1988). 'Calculation of the shape of the contact surface at Comet Halley,' *Ann. Geophys.* 88, 355–360.
85. Ytrehus, T., and Gjernes, E. (1988). 'Dusty Knudsen layers in cometary gas dynamics,' *Bulg. Acad. Sci. Theoretical and Applied Mechanics* 3, 99; also preprint (1989).